Coordination Chemistry Reviews 253 (2009) 647–665

Contents lists available at ScienceDirect

Coordination Chemistry Reviews

journal homepage: www.elsevier.com/locate/ccr

Review

The role of electronic delocalization in transition metal complexes from the electron localization function and the quantum theory of atoms in molecules viewpoints

Eduard Matito [a,*], Miquel Solà [b,**]

[a] *Lundbeck Foundation, Center for Theoretical Chemistry, University of Aarhus, 8000 Aarhus C, Denmark*
[b] *Institut de Química Computacional and Departament de Química, Universitat de Girona, Campus de Montilivi, s/n, 17071 Girona, Catalonia, Spain*

Contents

Abbreviations: 2c-2e, two-center two-electron bond; 3c-2e, three-center two-electron bond; 3c-4e, three-center four-electron bond; 5-MR, five-membered ring; 6-MR, six-membered ring; AO, atomic orbital; AOM, atomic overlap matrix; a.u., atomic units; B3LYP, Becke's three parameter nonlocal exchange and Lee–Yang–Parr 1988 nonlocal correlation functional; BP86, Becke's nonlocal exchange and Perdew 1986 nonlocal correlation functional; BCP, bond critical point; CCSD(T), coupled-cluster theory with singles and doubles and non-iterative estimation of triple excitations method; CASSCF, complete active space self-consistent field; DAFH, domain-averaged Fermi hole; DCD, Dewar–Chatt–Duncanson bonding model; DFT, density functional theory; DI, delocalization index; e, electrons; ELF, electron localization function; ESI, electron sharing index; FLU, aromatic fluctuation index; GC, guanine-cytosine base pair; H-bond, hydrogen bond; HF, Hartree–Fock method; HOMA, harmonic oscillator model of aromaticity; l.h.s., left hand side; LI, localization index; MCI, multicenter delocalization index; MO, molecular orbital; MSO, molecular spin–orbital; n-DI, n-center delocalization index; NBO, natural bond orbital; NICS, nucleus independent chemical shift; pd, pentadienylylidene; PDI, *para*-delocalization index; ptC, planar tetracoordinate carbon atom; QTAIM, quantum theory atoms in molecules; r.h.s., right hand side; RCP, ring critical point; TM, transition metal; TZP, triple-zeta plus polarization functions basis set; VSEPR, valence shell electron pair repulsion.

* Corresponding author. Tel.: +45 89423378.
** Corresponding author. Tel.: +34 972418912; fax: +34 972418356.
E-mail addresses: ematito@gmail.com (E. Matito), miquel.sola@udg.edu (M. Solà).

0010-8545/$ – see front matter
doi:10.1016/j.ccr.2008.10.003

ARTICLE INFO

Article history:
Received 23 April 2008
Accepted 2 October 2008
Available online 17 October 2008

Keywords:
Electronic delocalization
Electronic localization
Quantum theory of atoms in molecules (QTAIM)
Electron localization function (ELF)
Transition metal complexes

ABSTRACT

Electronic delocalization is invoked in many textbooks as the driving force of several fundamental phenomena such as conjugation, hyperconjugation, and aromaticity. These phenomena are important to explain structure, stability, and reactivity not only of classical organic compounds but also of many inorganic, organometallic, and all-metal cluster species. There are a number of available theoretical methods to quantify the electron localization/delocalization in molecules. In this review, we concentrate our efforts in the description of those studies that analyze electron delocalization in transition metal complexes employing the two most widespread techniques to measure delocalization: the electron localization function and the electron sharing indices obtained in the framework of the quantum theory of atoms in molecules. While the former enables the localization of regions in the molecular space where electrons concentrate leading to chemically significant regions such as bonds or lone pairs, the latter provides an atomic subdivision of the molecular space where each atom localizes a certain number of electrons. The joint effort of these techniques has already been proven as one of the most powerful methods to understand the chemical bonding. We show that theoretical studies of electron delocalization improve significantly our understanding of the bonding mechanism, structural properties, and reactivity of transition metal species.

1. Introduction

1.1. Importance of TM complexes

Living organisms transport and store transition metals (TMs). Although TM are present in small concentration ranges in biological systems, their importance is capital as they are bound to proteins or found in cofactors such as porphyrins or cobalamins. Iron, well-known for reversible binding of dioxygen (hemoglobin or hemerythrin), copper which participates in activation of dioxygen, cobalt found in vitamin B12 or molybdenum proteins catalyzing the reduction of nitrogen and nitrate are just a few examples which illustrate the importance of TM complexes in biological systems [1]. TMs are also important in a wide range of fields such as catalysis, material synthesis, photochemistry, bioinorganic chemistry and even cancer treatment, as is the case for *cis*-platinum which was shown, in 1965, to prevent cell division [2,3]. The synthesis of new TM complexes is timely and some complexes find striking applications, especially in the field of catalysis. In addition, TM complexes are appealing to the chemists due to the variety of colors exhibited in comparison with complexes formed by the main metals, which are usually white [4].

Due to the size and the number of electrons involved in TM complexes, reliable purely *ab initio* methods are prohibitive and the density functional theory (DFT) methods has had a prominent position in the understanding of TM chemistry [5]. Therefore, the role of the quantum chemistry in the field of TM chemistry has come along with the development of new functionals in the framework of DFT.

1.2. Chemical bonding in TM

TM complexes are species consisting of a TM covalently bonded (coordinated) to one or more molecules or ions (ligands). The formation of the complex can be understood as a Lewis acid, the TM cation, reacting with a Lewis base, the ligand.

The most successful simple model to explain the chemical bonding is perhaps the electron pairing model developed by Lewis, who in addition to his cubic atom theory, gave rise to the well-known octet rule [6]. The octet rule is a rule of thumb which states that atoms tend to combine in such a way that they occupy their valence shells with eight electrons. In TM chemistry there is an analogy to the octet rule, the 18-electron rule, which is used for characterizing and predicting the stability of metal complexes. The origin of this rule comes from the fact that valence shells of a TM can accommodate 18 electrons: 2 in each of the five d orbitals, 2 in each of the three p orbitals and 2 in the s orbital.

In as much as several quantum mechanical concepts such as the electron sharing indices (ESI) [7] or bond orders [8–10] have overcome the octet rule to analyze chemical bonding, several theories have also been defined to improve the picture of the chemical bonding in TM chemistry provided by the Lewis model. The ligand field theory (LFT) is one of the most widely used models, still present in most textbooks that analyze TM chemistry. LFT represents an application of molecular orbital theory (MOT) to TM complexes, and is an improvement over the well-known crystal field theory (CFT), which uses an electrostatic model to explain all metal ion–ligand interactions and was first proposed by Hans Bethe in 1929 [11].

Several quantum chemical tools have been designed to analyze chemical bonding, including the natural bond orbital (NBO) methods [12], the charge decomposition (CDA) [13] or the energy-decomposition analyses (EDA) [14]. For a recent review on the nature of bonding covering some of these aspects in TM compounds see Ref. [15]. The aim of this review is to pursue the study in TM bonding by focusing on the electron delocalization in TM species. Namely, we will analyze the role of two quantum chemical tools, the quantum theory of atoms in molecules (QTAIM) and the electron localization function (ELF), to have a good grasp of the electron delocalization in TM chemistry. We will show through a series of examples how these two approaches can be successfully used to analyze the most fascinating bonding situations encountered in TM chemistry.

1.3. QTAIM and ELF, competing or complementing each other?

Since the appearance of the ELF in the literature in 1990, several researchers [16–19] have deeply analyzed the differences between QTAIM and ELF approaches. So far, the QTAIM has been the preferred quantum mechanical tool to analyze chemical bonding and chemical interactions.

QTAIM, based on the topology of the electron density, enables the partition of the molecular space into atomic regions, giving rise to atomic properties including the atomic population and its statistical interpretation accompanying, as well as a bunch of chemical tools which were used to analyze the chemical bonds: the bond critical point (BCP) and the ring critical point (RCP), the value of the density, the energy density and the Laplacian of the electron density calculated in these points are just a few examples. QTAIM was not exempt of controversy, and some of the issues of the theory, such as the tenet [20] that a BCP and a bond path connecting two

Table 1
B3LYP calculation for $Cr(CO)_6$ and CO (6-31G(d,p) basis set for C and O and Roos [185] augmented Double Zeta ANO for Cr). Density values ($\rho(\mathbf{r_{bcp}})$), Laplacian of the density values ($\nabla^2\rho(\mathbf{r_{bcp}})$), ratio values between the perpendicular and the parallel curvatures ($|\lambda_1|/\lambda_3$), and local energy density ($H(\mathbf{r_{bcp}})$) at the different critical points in the molecule. All quantities are given in a.u.

Molecule	bcp	$\rho(\mathbf{r_{bcp}})$	$\nabla^2\rho(\mathbf{r_{bcp}})$	ε	λ_1	λ_2	λ_3	$\lvert\lambda_1\rvert/\lambda_3$	$H(\mathbf{r_{bcp}})$
$Cr(CO)_6$	Cr–C	0.1071	0.4849	0.0000	−0.0940	−0.0940	0.6730	0.1397	−0.0297
	C–O	0.4615	0.9937	0.0000	−1.3908	−1.3908	3.7753	0.3684	−0.7747
CO	C–O	0.4712	1.3545	0.0000	−1.5510	−1.5510	4.4566	0.3480	−0.7701

atomic basins is actually a sufficient condition for the existence of a chemical bond, have been repeatedly debated [20–33]. The quantities discussed in this review to analyze electronic localization/delocalization do not suffer from the criticism exerted on the interpretation of BCPs and bond paths in QTAIM theory, since the QTAIM framework is only used as a way to partition the molecular space to compute $S_{ij}(A)$ values (*vide infra*).

The ELF represents a quite different approach to the analysis of the chemical bonding. In like manner to QTAIM, the ELF also tackles the topology of a function in order to analyze the molecular space, but it does not use the electron density itself but the conditional probability for the same spin pairs (*vide infra*). It provides us with a division of the molecular space, but the different pieces (basins) arising from this decomposition are not necessarily attached to a given atom, and usually have some chemical significance like bonding regions, lone pairs or core basins. The population of these basins likewise gives rise to a statistical analysis which, as we will shortly see, allows for the interpretation of the molecule in terms of mesomeric structures.

To put it in a nutshell, ELF have some similar features to QTAIM but generally allows for a completely different approach to the chemical bonding. Usually the interpretation gathered coincides, and one complements the other, as QTAIM provides with an atomic partition which generates atomic domains, whereas ELF shows localization domains and its partition allows for the calculation of properties in particularly interesting chemical regions [34,35]. Moreover, the superposition of both topologies shows where a particular bonding region (or in general any basin obtained with the ELF partition) is located with respect to the atom boundaries provided by the QTAIM. This technique has been used, among other things, to decide about bond polarization. Notwithstanding, as we have already shown [18], sometimes they provide different, if not contradictory, pictures of the chemical bond. In this sense, one should step carefully when interpreting the results arisen from these methods.

This review is organized as follows. In the next two sections, we will explain the theoretical basis for these two approaches. In order to illustrate the procedure by which the different features arising from this analysis explain the chemical bonding, we have chosen a very simple molecule, $Cr(CO)_6$, to serve as an example. Section 4 contains a series of examples carefully extracted from the literature in order to cover a wide range of different chemical situations given in TM chemistry where QTAIM and ELF have been analyzed at some extent. Section 5 summarizes the conclusions.

2. The atoms in molecules approach to electron delocalization

The quantum theory of atoms in molecules (QTAIM) analyzes the topology of the molecular one-electron density and, from this analysis, it provides a wide set of concepts useful to characterize electronic structure such as atomic populations and charges, measures of electronic localization and delocalization (through the so-called localization and delocalization indices, $\delta(A,B)$, *vide infra*), properties of critical points like BCPs or RCPs (electron density, ellipticity, Laplacian and local energy density, among others), and many others [36–39]. In the QTAIM, the Laplacian of the one-electron density ($\nabla^2\rho(\mathbf{r})$), which is obtained as the trace of the Hessian matrix, is one of the tools most extensively used to analyze electron delocalization. The electronic charge is locally concentrated within a molecular system in regions where $\nabla^2\rho(\mathbf{r}) < 0$. Indeed, local maxima of the negative of this quantity ($-\nabla^2\rho(\mathbf{r})$) denote spatial domains where local electron pairing takes place providing a physical basis for the Lewis and VSEPR models [20,36–38,40–43]. Some authors have also used the ellipticity profile along the bond path to discuss delocalization [44,45]. The ellipticity (ε) is a measure of the cylindricity of the charge distribution and is calculated as $\varepsilon = \lambda_1/\lambda_2 - 1$ (with $\lambda_1 < \lambda_2 < 0$), λ_i being the eigenvalues of the corresponding eigenvectors of the Hessian matrix of $\rho(\mathbf{r})$ perpendicular to the bond path. Values of ε greater than zero may indicate, for instance, partial π-character in a bond or the presence of agostic interactions [45]. On the other hand, local energy density, which is calculated as the sum of the local kinetic plus potential energy, $\mathbf{H}(\mathbf{r}) = \mathbf{V}(\mathbf{r}) + \mathbf{K}(\mathbf{r})$, is used to decide about the covalency of the bond into question; $H(r) < 0$ is usually given in covalent interactions while $H(r) > 0$ for ionic ones.

Table 1 collects the aforementioned data for $Cr(CO)_6$ and CO (see also Ref. [46] for a detailed discussion). Values of $|\lambda_1|/\lambda_3 < 1$, $\rho(\mathbf{r_{bcp}})$ small, $\nabla^2\rho(\mathbf{r_{bcp}}) > 0$ and small $\delta(A,B)$ are typical of closed-shell interactions such as ionic, hydrogen bonds, or van der Waals interactions, while $|\lambda_1|/\lambda_3 > 1$, $\rho(\mathbf{r_{bcp}})$ large, $\nabla^2\rho(\mathbf{r_{bcp}}) < 0$ and large $\delta(A,B)$ correspond to covalently shared interactions. On the other hand, metal–metal bonds are characterized by similar values to those found for ionic interactions, except for the fact that delocalization indices are much larger in metallic than ionic interactions [46]. The CO molecule has a very special electron density as a result of the charge transfer from C to O and a large opposing polarization due to the positive charge on C [47]. As a result, the value of the Laplacian at the BCPs in Table 1 is positive, indicating electron depletion, particularly large at the C–O bonding, but values of $\rho(\mathbf{r_{bcp}})$ and δ(C,O) (see Table 2) are quite large, so it must be considered a shared interaction corresponding to a covalent polar bond [46]. All the values are very similar for free CO and CO in $Cr(CO)_6$ excepting for the Laplacian which is slightly greater in free CO, indicating a higher depletion in carbon monoxide. The value of the density is small in the Cr–C BCP and the ratio between the eigenvalues $|\lambda_1|/\lambda_3$ for Cr–C is also typical of closed-shell dative

Table 2
B3LYP calculation for $Cr(CO)_6$ and CO (6-31G(d,p) basis set for C and O and Roos [185] augmented Double Zeta ANO for Cr). QTAIM basin (N), electronic charge (q), localization index (λ), percentage of localization with respect to population basin (%λ) and electron sharing indices ($\delta(A,B)$) for $Cr(CO)_6$. All quantities are given in a.u.

Molecule	Atom	N	q	λ	%λ	Pair	$\delta(A,B)$
$Cr(CO)_6$	Cr	22.8027	1.1973	19.9106	87.32	Cr,C	0.8172
	C	4.9947	1.0053	3.5525	71.13	C,O	1.5436
	O	9.2042	−1.2042	8.3000	90.18		
CO	C	4.7784	1.2216	3.9135	81.90	C,O	1.7262
	O	9.2216	−1.2216	8.3585	90.64		

interactions. The eigenvalues of the Hessian are degenerate due to the symmetry of the molecule, and thus the ellipticity is zero, for both BCPs. The value of the energy density at the BCP is negative for both compounds, indicating that the local potential energy ($\mathbf{V}(\mathbf{r})$) partly predominates over the local kinetic energy ($\mathbf{K}(\mathbf{r})$); as is the case for shared interactions, the value is specially large for C–O. Overall, Cr–C presents the typical signature of a closed-shell dative (or semipolar) interaction, on the other hand, C–O presents similar features to those found in free CO.

Both, the Laplacian and the ellipticity are properties based on the one-electron density. However, since the electron pair formation [48] depends on the probability of finding two electrons simultaneously at two positions close in space, most methods used to determine electronic localization/delocalization are based on the two-electron density or pair density [49–52], $\gamma^{\sigma_1\sigma_2}(\vec{r}_1, \vec{r}_2)$, which is the simplest quantity that describes the electron pair behavior. The pair density can be interpreted as the probability density of two electrons being simultaneously at positions $\vec{r}_1$ and $\vec{r}_2$ with spins σ_1 and σ_2, respectively, regardless of the position of the other $N-2$ electrons. Thus, $\gamma^{\sigma_1\sigma_2}(\vec{r}_1, \vec{r}_2)$ is the natural function to examine very relevant quantum chemical phenomena such as the electron correlation effects or the formation of localized α, β pairs. After spin integration of $\gamma^{\sigma_1\sigma_2}(\vec{r}_1, \vec{r}_2)$, one gets the spinless pair density, which can be split into an uncorrelated pair density part and a part that gathers all exchange and correlation effects

$$\gamma(\vec{r}_1, \vec{r}_2) = \rho(\vec{r}_1)\rho(\vec{r}_2) + \gamma_{xc}(\vec{r}_1, \vec{r}_2). \tag{1}$$

The uncorrelated part of the pair density, given by the product $\rho(\vec{r}_1)\rho(\vec{r}_2)$, provides the probability density of finding simultaneously two independent electrons at positions $\vec{r}_1$ and $\vec{r}_2$; it can be considered as a *fictitious pair probability* which allows for two particles to be located in the same position. The difference between $\gamma(\vec{r}_1, \vec{r}_2)$ and $\rho(\vec{r}_1)\rho(\vec{r}_2)$ is the exchange-correlation density, $\gamma_{xc}(\vec{r}_1, \vec{r}_2)$, which is a measure of the degree to which density is excluded at $\vec{r}_2$ because of the presence of an electron at $\vec{r}_1$. Given the fact that the one-electron density and the pair density are normalized to N electrons and $N(N-1)$ electron pairs, respectively, the double integration of the exchange-correlation density, as defined in Eq. (1), yields $-N$ electrons, corresponding to the number of autopairs contained in this fictitious pair density, $\rho(\vec{r}_1)\rho(\vec{r}_2)$. By dividing $\gamma(\vec{r}_1, \vec{r}_2)$ by $\rho(\vec{r}_1)$ one gets the so-called conditional pair density, $P(\vec{r}_1, \vec{r}_2)$, which gives the probability of observating an electron at position $\vec{r}_2$ when one electron is known to be at reference position $\vec{r}_1$:

$$P(\vec{r}_1, \vec{r}_2) = \frac{\gamma(\vec{r}_1, \vec{r}_2)}{\rho(\vec{r}_1)}. \tag{2}$$

Since $\gamma(\vec{r}_1, \vec{r}_2)$ can be further partitioned in same spin and unlike spin electron contributions:

$$\gamma(\vec{r}_1, \vec{r}_2) = \gamma^{\alpha\alpha}(\vec{r}_1, \vec{r}_2) + \gamma^{\alpha\beta}(\vec{r}_1, \vec{r}_2) + \gamma^{\beta\alpha}(\vec{r}_1, \vec{r}_2) + \gamma^{\beta\beta}(\vec{r}_1, \vec{r}_2), \tag{3}$$

it is possible to write the $P^{\sigma\sigma}(\vec{r}_1, \vec{r}_2)$ and $P^{\sigma\sigma'}(\vec{r}_1, \vec{r}_2)$ contributions to the conditional pair density as

$$P^{\sigma\sigma}(\vec{r}_1, \vec{r}_2) = \rho^{\sigma}(\vec{r}_2) + \rho_{xc}^{\sigma\sigma}(\vec{r}_1, \vec{r}_2), \tag{4}$$

$$P^{\sigma\sigma'}(\vec{r}_1, \vec{r}_2) = \rho^{\sigma'}(\vec{r}_2) + \rho_{xc}^{\sigma\sigma'}(\vec{r}_1, \vec{r}_2). \tag{5}$$

In Eqs. (4) and (5), the $\rho_{xc}^{\sigma\sigma}(\vec{r}_1, \vec{r}_2)$ and $\rho_{xc}^{\sigma\sigma'}(\vec{r}_1, \vec{r}_2)$ ($\sigma = \alpha, \beta$) terms are the so-called Fermi and Coulomb holes. The Fermi hole is a non-positive quantity determining the decrease in the probability of finding another electron with the same spin relative to a fixed position of the electron of reference located at $\vec{r}_1$. Its integral over $\vec{r}_2$ equals -1, corresponding to the removal of a same-spin electron from the σ-spin density, $\rho^{\sigma}(\vec{r}_2)$. Bader and Stephens [53,54] showed that the extent of localization or delocalization of an electron of reference is determined by the corresponding localization of its Fermi hole [48]. Accordingly, Fermi hole density maps have been employed to discuss electronic delocalization [55–59]. Other related quantities are the localization and delocalization indices (LIs and DIs) defined by Bader and coworkers [54,60,61] within the framework of the QTAIM [36–38,62]. These indices are obtained by the double integration of the exchange correlation density (the sum of the Fermi and Coulomb holes weighted by the density of the reference electron) [49,50] over the atomic domain.

$$\lambda(A) = -\int_A \int_A \gamma_{xc}(\vec{r}_1, \vec{r}_2)\, \mathrm{d}\vec{r}_1\, \mathrm{d}\vec{r}_2, \tag{6}$$

$$\delta(A, B) = -2\int_B \int_A \gamma_{xc}(\vec{r}_1, \vec{r}_2)\, \mathrm{d}\vec{r}_1\, \mathrm{d}\vec{r}_2. \tag{7}$$

The DI [60], $\delta(A,B)$, more generally known as electron sharing index (ESI) [7], gives a quantitative measure of the number of electron pairs delocalized or shared between atomic basins A and B, while the LI [60], $\lambda(A)$, is a measure of the average number of electrons localized on atom A.

Let us briefly mention here that single instead of double integration of the exchange correlation density in a given domain gives rise to the domain-averaged Fermi holes (DAFH) [65], which have been used by Ponec and coworkers to locate electron pairs, visualize chemical bonds, and analyze its nature [63–70].

Eqs. (6) and (7) require integration over atomic domains. In the QTAIM, these domains are the *atomic basins* [36–39] defined as the regions in real space bound by zero-flux surfaces in $\rho(\vec{r})$ or by infinity.[1] Usually each basin contains an atomic nucleus, which acts as a topological attractor for the basin. Thus, each non-overlapping and non-spherical basin is assigned to one of the atoms in a molecule. This partitioning scheme ensures that each atomic subsystem behaves as a proper open system. Moreover, the atomic contributions to any molecular property can be calculated by integration of the proper operator through the atomic basins. For instance, the electron population of an atom A is defined as follows:

$$N(A) = \int_A \rho(\vec{\mathbf{r}})\, \mathrm{d}\vec{\mathbf{r}}, \tag{8}$$

where the subscript A indicates that the integration has to be carried out only through the space corresponding to the atomic basin of atom A. From the electron population one may obtain the atomic charge subtracting the atomic number: $q(A) = Z(A) - N(A)$. The atomic properties obtained in this way are additive, summing to the corresponding values for the total system. Thus, summation of all the atomic populations in a molecule yields the total number of electrons, N. The following sum rule can be easily demonstrated:

$$N(A) = \lambda(A) + \frac{1}{2}\sum_{B \neq A} \delta(A, B). \tag{9}$$

Eq. (9) proves that the total number of electrons belonging to a given atomic domain can be exactly partitioned into its localized, $\lambda(A)$, and delocalized, $1/2\sum_{B \neq A}\delta(A, B)$, parts. It is also customary to provide the percentage of electron localization in a given basin, calculated as the ratio $\%\lambda(A) = 100 \times \lambda(A)/N(A)$.

Table 2 contains the integrated quantities for $Cr(CO)_6$ and CO. The charge on C atom decreases by about 0.2 e when going from free CO to the $Cr(CO)_6$ complex. Let us note in passing that atomic charges are not absolute values and that different atomic charge

[1] In calculations a threshold on the value of the density is used to find the *practical* limits of the atomic basins.

methods have different scales and yield different values for the same compound [71]. Neither the values of the charge nor the delocalization indices found for oxygen atoms vary when CO coordinates to Cr. The value of 1.544 e for the DI between C and O is slightly smaller to that found in free carbon monoxide (1.726 e at the B3LYP/6-31g(d,p) level). The reduction in the number of delocalized electrons (0.178 e) between C–O does not correspond to an increase in the electrons localized in the C basin, which remain practically constant. Instead, they delocalize towards Cr, as suggested by the lower electron localization (11%) of carbon basin in the complex and the significant electron sharing between Cr and C (DI amounts 0.817 e). This reorganization is already expected taking into account the fact that the bonding between the CO and the complex follows the well-known Dewar–Chatt–Duncanson (DCD) scheme [72,73], with σ-donation from the CO π orbital to an unoccupied d orbital of the metal and backdonation from an occupied d orbital of the metal to the π* orbital of CO.

The calculation of LIs and DIs can also be done using other partitions, like the Mulliken-like partitioning in the Hilbert space spanned by the basis functions or the fuzzy-atom approach [74] and, in many cases, one obtains similar values to those provided by integration over QTAIM atomic domains [75,76].

Eqs. (6)–(9) can be applied at any level of theory, provided that the first and second-order density functions are known. For TM species, the calculation of LIs and DIs is usually carried out with the DFT approach using the approximate wave function derived from Kohn–Sham orbitals [77]. In this case, as well as at the Hartree–Fock (HF) level, the expressions for the LI and DI are written as

$$\lambda(A) = \sum_{i,j} (S_{ij}(A))^2, \tag{10}$$

$$\delta(A,B) = 2\sum_{i,j} S_{ij}(A) S_{ij}(B), \tag{11}$$

where $S_{ij}(A)$ stands for the atomic overlap matrix (AOM) of atom A (overlap between molecular orbitals integrated within the basin of atom A) and the summations run over all occupied molecular spin–orbitals (MSOs) in the molecule. The quantity $V(A) = \sum_{B\neq A}\delta(A,B) = 2[N(A) - \lambda(A)]$ is taken as a measure of number of electrons on A that are delocalized over other atoms. At the HF and DFT levels, LIs and DIs in Eqs. (10) and (11) reduce to Wiberg indices if integrations over atomic basins are replaced by a Hilbert space partitioning of the corresponding integrals. The AOMs in Eqs. (10) and (11) that are needed to compute LIs and DIs and can be obtained using different programs, among them the AIMPAC [78], AIM2000 [79–81], MORPHY98 [82–84], XAIM [85], TOPOND [86], and GAUSSIAN98 suites of programs [87].

The definition of DI can be generalized to study multicenter bonding. It is possible to define a multicenter DI [88,89] between the N centers A_1 to A_N. Let us consider a ring structure of N atoms represented by the following string $A = \{A_1, A_2, \ldots, A_N\}$, whose elements are ordered according to the connectivity of the atoms in the ring. The closed-shell form of this index at the HF or DFT level is given by:

$$I_{ring}(\mathcal{A}) = 2^N \sum_{i_1,i_2,\ldots,i_N}^{occ.MO} S_{i_1 i_2}(A_1) S_{i_2 i_3}(A_2) \ldots S_{i_N i_1}(A_N), \tag{12}$$

where the internal summation run over all occupied molecular orbitals (MOs).

Bultinck and coworkers have proposed an alternative to the I_{ring} index: summing up all the I_{ring} values resulting from the permutations of indices A_1, A_2, …, A_N to define the multicenter index, whose formula reads:

$$MCI(\mathcal{A}) = \frac{1}{2N}\sum_{P(A)} I_{ring}(\mathcal{A}), \tag{13}$$

where $P(\mathcal{A})$ represents all possible permutations between centers A_1 to A_N. The reader may easily prove that MCI [88,89] and I_{ring} provide the same values for three-membered rings, since permutation of three elements keep the connectivity between them. These definitions are ring size-dependent, and recently we recommended a normalization of Eqs. (12) and (13) which provides values closely matching the topological resonance energies per π-electron [90].

Several other measures of aromaticity have been proposed based on the DIs, among them we can cite PDI [91], FLU [92], MCI [93], I_{NB} or I_{NG} [90]. For a critical assessment of this and other measures of aromaticity see Refs. [94] and [95]. The DIs and LIs as well as FLU, PDI, I_{ring}, and MCI indices can be calculated from the AOMs by means of the ESI-3D program [96].

One of the aims of this review is to illustrate with some representative examples the utility of the electron localization/delocalization analysis in the framework of the QTAIM for the description of chemical structure, molecular bonding, and reactivity. As said before, the QTAIM provides different tools for the characterization of the chemical bonding; however we will concentrate on those concerning the analysis of electron localization/delocalization. Namely, in this work the usage of the atoms in molecules (AIM) theory of Bader mainly concentrates in the use of AIM atomic partition defined from the condition of zero-flux gradient in the one-electron density to compute $S_{ij}(A)$ values. However, as said before [75,76], other partitions of the molecular space can also be used. In the following, we restrict the QTAIM papers in the review to those studies that use LIs and DIs obtained from the second-order density to discuss electron localization/delocalization in molecules containing TM. Complementary reviews on this topic and related issues can be found in Refs. [46,97–99].

3. Electron localization function

3.1. Introduction

Nowadays one of the most widely used quantum-mechanical tools to analyze electron localization is probably the electron localization function (ELF). The ELF was introduced by Becke and Edgecombe from the leading term in the Taylor series expansion of the spherically averaged same-spin conditional pair probability [98,100–103], Eq. (4). The conditional probability presents a clear advantage over the pair density: it contains all relevant information about the motion of pairs of electrons as the pair density does, while it does not contain irrelevant information concerning the position of the reference electron **1**. Becke and Edgecombe [100] took the spherical average of the conditional probability for *same spin* electrons:

$$\begin{aligned}\langle e^{\vec{s}\cdot\vec{\nabla}} P^{\sigma\sigma}(\vec{r},\vec{r}+\vec{s})\rangle &= \frac{1}{4\pi}\left(\int_{-1}^{1}\int_{0}^{2\pi} e^{s\nabla\theta}\,\mathrm{d}\theta\,\mathrm{d}\phi\right) P^{\sigma\sigma}(\vec{r},\vec{r},+\vec{s})|_{\vec{s}=0} \\ &= \frac{\sinh(s\nabla)}{s\nabla} P^{\sigma\sigma}(\vec{r},\vec{r}+\vec{s})|_{\vec{s}=\vec{0}},\end{aligned} \tag{14}$$

and expanded it by series of Taylor around the position of the reference electron [104]:

$$\begin{aligned}\langle e^{\vec{s}\cdot\vec{\nabla}} P^{\sigma\sigma}(\vec{r},\vec{r}+\vec{s})\rangle &= \left(1 + \frac{1}{6}s^2\nabla_s^2 + \cdots\right) P^{\sigma\sigma}(\vec{r},\vec{r},+\vec{s})|_{\vec{s}=\vec{0}} \\ &\approx \frac{1}{6}s^2\nabla_s^2 P^{\sigma\sigma}(\vec{r},\vec{r}+\vec{s})|_{\vec{s}=\vec{0}},\end{aligned} \tag{15}$$

The r.h.s. of Eq. (15) holds because the same spin pair density at the coalescence point is zero, $\gamma^{\sigma\sigma}(\mathbf{r},\mathbf{r})=0$, as stated by Pauli principle.

Becke and Edgecombe [100] used a function proportional to the leading term of the Taylor expansion of the spherically averaged same-spin conditional pair probability:

$$D_\sigma = \frac{1}{2}\nabla_s^2 P^{\sigma\sigma}(\vec{r},\vec{r}+\vec{s})|_{\vec{s}=\vec{0}}, \tag{16}$$

and calculated the relative ratio with respect to the same quantity for the homogenous electron gas, D_σ^0, for a monodeterminantal wave function (where the pair density can be calculated straightforwardly from the density) [105]:

$$D(\vec{r}) = \frac{D_\sigma}{D_\sigma} = \left.\frac{\langle e^{\vec{s}\cdot\vec{\nabla}} P^{\sigma\sigma}(\vec{r},\vec{r}+\vec{s})\rangle/(s^2/3)}{3/5(6\pi^2)^{2/3}[\rho^\sigma(\vec{r})]^{5/3}}\right|_{\vec{s}=\vec{0}}$$
$$= \frac{\nabla_s^2 \gamma^{(2)\sigma\sigma}(\vec{r},\vec{r}+\vec{s})|_{\vec{s}=\vec{0}}}{c_F[2\rho^\sigma(\vec{r})]^{8/3}}, \tag{17}$$

where the c_F is the Fermi constant.

The probability of observation an electron with spin σ when there is already another electron with the same spin nearby is lower when the former is localized. Therefore, the ratio in Eq. (17) accounts for electron localization; the higher it is, the lower the localization. The ELF was defined as a function of the aforementioned ratio in order to range the electron localization measure in the interval [0,1] [100]:

$$ELF = \eta = \frac{1}{1+D(\vec{r})^2} = \frac{1}{1+(D_\sigma/D_\sigma^0)^2}, \tag{18}$$

ELF = 1 corresponds to a completely localized situation, 0 to corresponds to a delocalized system, and ELF = 0.5 is the value one should obtain for the homogenous electron gas.

The original definition of the ELF was developed for a monodeterminantal wave function, and thus Eq. (17) was further simplified by expanding the pair density in terms of the first-order density matrix. In the present development we have preferred not expanding the pair density, so that the ELF definition is general for any method which has the pair density available. Unfortunately the exact expression of the pair density for the homogenous electron gas remains unknown (to be the best of our knowledge) and thus the ELF definition is not general in this respect. However, Silvi [106] and Kohout [107] independently demonstrated that ELF expression might be derived without any need of using the homogenous electron gas as a reference. Indeed, we already proved that their expressions, and those developed by Dobson [108,109] are equivalent [110]. For a recent review on the limits of the ELF see Ref. [111].

The ELF has also been calculated separately for alpha and beta orbitals with the aim to study different spin contributions on some radical systems [112]. The ELF has been successfully used to gain inside on aromaticity [98,113,114], to analyze the changes in electronic structure along a given reaction coordinate [115,116] and to distinguish between similar mechanisms of reaction [117,118], among other things.

3.2. Topology of the ELF

The most attractive feature of the ELF comes from its graphical representation. The ELF provides a nice picture of the electronic structure in molecules [119], by showing the regions of the molecular space where electrons localize. The local maxima of ELF define *localization domains*. In contrast with QTAIM, the domains do not correspond to atoms in the molecule, but to chemically interesting regions. Namely, three different domains are obtained from the ELF partition of the molecular space: bonding and non-bonding valence domains (usually corresponding to bonds and lone pairs respectively) and core basins [103]. The spatial organization of localization domains will provide with the classification of the chemical bonds. Namely, the synaptic order, or the number of atoms to which a given basin is bounded, determinates the nature of the basin in question.

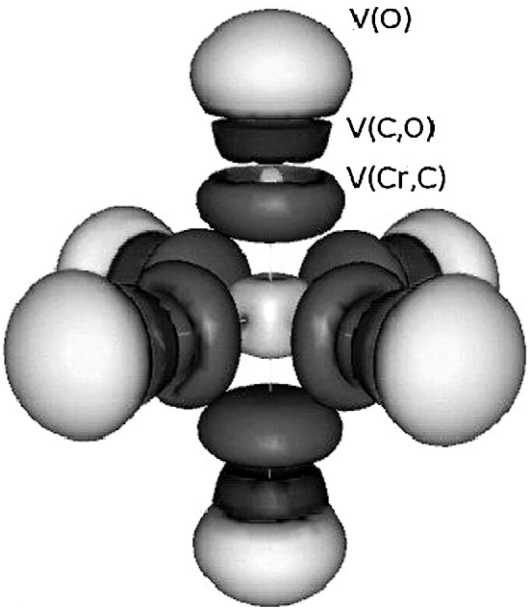

Fig. 1. ELF = 0.60 isosurface for $Cr(CO)_6$ (B3LYP calculation with 6-31G(d,p) basis set for C and O and Roos [185] augmented Double Zeta ANO for Cr). The valence basins for oxygen, carbon and chromium are indicated.

The ELF reproduces to some extent the shell structure of atoms [120,121], and unlike other quantities which account for the electron localization such as the Laplacian of the electron density [122,123,124], the ELF also provides a good estimation of the number of electrons per atomic shell (shell numbers). However, as we have recently proven [110], even for correlated wavefunctions the ELF is not able to recover the shell numbers for TM atoms. Especially difficult to recover are outer shells such as *M* or *N*; for such atoms their configuration is no longer exclusively ruled by the Aufbau principle, and Hund's rule plays a prominent role [110].

Fig. 1 displays the isosurface ELF = 0.60 for $Cr(CO)_6$. The higher the ELF value, the easier to identify the basins. In the picture we may see the valence basin associated with the oxygen atom lone pair, V(O), the carbon and oxygen bonding basins, V(C,O) and chromium valence basin V(C,Cr). Between V(C,O) basin and V(C,Cr) one can see the carbon core C(C) basin, and in the center of the axis the core basin associated with chromium pops up. Examining the picture we may already extract a conclusion about the bonding in $Cr(CO)_6$. The disynaptic character of the bonding basin, V(C,Cr), seems to suggest that there is a shared interaction between C and Cr, however according to the distance between V(C,Cr) and the core basins C(C) and C(Cr) this is a rather closed-shell interaction. Further analysis on the correlation between these basins might shed some more light in this issue.

3.3. Bifurcation analysis

The topology of ELF provides localization domains. When such domains are studied for a given reaction we may follow a reaction mechanism as a series of topological changes occurring along the

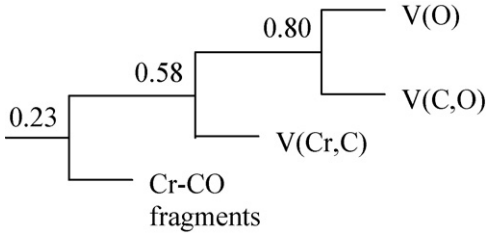

Fig. 2. ELF bifurcation diagram for $Cr(CO)_6$.

reaction path. The changes in the topology, such as the breaking or joining of basins, are restricted by the mathematical condition of Poincaré-Hopf.

In order to define a hierarchy of localization basins, the concept of localization domain was introduced [125]. A localization domain is a volume limited by one or more isosurfaces and containing at least one attractor. If the domain contains only one attractor it is called irreducible, otherwise reducible. Increasing the value of the ELF isosurface reducible domains *reduce* to smaller reducible or irreducible domains. Such reduction occurs at the turning points, critical points located at the separatrix of the two basins involved in the parent domain. This turning might be ordered by increasing value of ELF providing a hierarchy diagram or bifurcation diagram. This diagram gives a clear picture of how the domains localize from groups of basins to individual basins.

Fig. 2 depicts the bifurcation diagram for $Cr(CO)_6$. For values greater than ELF = 0.23 the different Cr–CO fragments separate from each other, as one would expect since each CO barely interacts with the others. At ELF = 0.58 V(Cr,C) separates from the pattern domain, pinpointing the closed-shell character of C–Cr interaction. On the contrary, C–O covalent bond separates into V(O) and V(C,O) when ELF reaches the high value of 0.80.

3.4. Statistical interpretation of the electron density in ELF domains

The partition of the molecular space enables basin-related properties to be calculated by integrating the density of a certain property over the volume of the basins. Thus, for a basin labeled Ω_i, one can define the average population as:

$$\bar{N}(\Omega_i) = \int_{\Omega_i} \rho(\vec{r})\,\mathrm{d}\vec{r}, \tag{19}$$

and its variance:

$$\begin{aligned}\sigma^2(\Omega_i) &= \langle (N(\Omega_i) - \bar{N}(\Omega_i))^2 \rangle \\ &= \int_{\Omega_i} \gamma^{(2)}(\vec{r}_2, \vec{r}_2)\,\mathrm{d}\vec{r}_1\,\mathrm{d}\vec{r}_2 - \bar{N}(\Omega_i)[\bar{N}(\Omega_i) - 1].\end{aligned} \tag{20}$$

The variance of the basin population is a measure of the quantum mechanical uncertainty of the basin population, which can be interpreted as a consequence of the electron delocalization. One can also define likewise the pair population:

$$N(\Omega_i, \Omega_j) \equiv \langle N(\Omega_i) \cdot N(\Omega_j) \rangle = \int_{\Omega_i}\int_{\Omega_j} \gamma^{(2)}(\vec{r}_1, \vec{r}_2)\,\mathrm{d}\vec{r}_1\,\mathrm{d}\vec{r}_2, \tag{21}$$

The variance, $\sigma^2(\Omega_i)$, can also be split in terms of contributions from other basins,

$$\sigma^2(\Omega_i) = -\sum_{j\neq i} V(\Omega_i, \Omega_j), \tag{22}$$

where $V(\Omega_i, \Omega_j)$ is the population covariance, and is calculated as follows:

$$\begin{aligned} V(\Omega_i, \Omega_j) &= \langle N(\Omega_i) \cdot N(\Omega_j) \rangle - \langle N(\Omega_i) \rangle \langle N(\Omega_j) \rangle \\ &= \int_{\Omega_i}\int_{\Omega_j} (\gamma^{(2)}(\vec{r}_1, \vec{r}_2) - \rho(\vec{r}_1)\rho(\vec{r}_2))\,\mathrm{d}\vec{r}_1\,\mathrm{d}\vec{r}_2 \\ &= \int_{\Omega_i}\int_{\Omega_j} (\gamma_{xc}(\vec{r}_1, \vec{r}_2))\,\mathrm{d}\vec{r}_1\,\mathrm{d}\vec{r}_2 \end{aligned} \tag{23}$$

Inspection of Eqs. (23) and (7) gives another interpretation for the DI. It is actually proportional to the covariance of the populations of the two atoms involved. Both quantities, the covariance of the populations between ELF domains and the DI between two given atoms, account for the correlative interactions between two given regions of the molecular space, but due to the different nature of the partitioning of the molecular space, the resulting quantities are not same.

The *relative fluctuation* measures the ratio of electrons delocalized in a given basin with respect to the population of that basin. This quantity, which is non-negative defined, gives a percentage of electron delocalization in a given basin:

$$\lambda_F(\Omega_i) = \frac{\sigma^2(\Omega_i)}{\bar{N}(\Omega_i)} \cdot 100 = \frac{\bar{N}(\Omega_i) - \lambda(\Omega_i)}{\bar{N}(\Omega_i)} \cdot 100, \tag{24}$$

where $\lambda(\Omega_i)$ has the same significance than in Eq. (6) but applied to an ELF basin.

In order to estimate the importance of a given interaction between a pair of basins with respect to the number of electrons delocalized in that basin, one can calculate the contribution analysis (CA) which reads as follows:

$$CA(\Omega_i|\Omega_j) = \frac{V(\Omega_i, \Omega_j)}{\sum_{k\neq j} V(\Omega_j, \Omega_k)} \cdot 100 = \frac{-V(\Omega_i, \Omega_j)}{\sigma^2(\Omega_j)} \cdot 100, \tag{25}$$

Finally, the integrated spin density may also be important for open-shell systems:

$$S_z(\Omega_i) = \int_{\Omega_i} [\rho^\alpha(\vec{r}_1) - \rho^\beta(\vec{r}_1)]\,\mathrm{d}\vec{r}_1. \tag{26}$$

Table 3 collects the values for some of the functions aforementioned. The core basins of C and O only contain the $1s^2$ core electrons which are highly localized and thus the contribution analysis is irrelevant for these basins. The chromium core basin is however more spread and correlated with valence basins V(Cr,C) as expected for TM which locate electrons in more delocalized orbitals. V(O) contains the lone pair of oxygen and is highly correlated with the V(C,O) basin. On the other hand, V(C,O) holds an average of 3.12 e, suggesting a triple bond highly polarized towards oxygen as one may deduce for its high relative fluctuation, whose main contribution comes from V(O) basin. The bonding between Cr and C can be studied for the parameters of V(Cr,C) basin. Despite the fact the basin holds an average of 2.76 electrons, these electrons are highly

Table 3
B3LYP calculation for $Cr(CO)_6$ (6-31G(d,p) basis set for C and O and Roos [185] augmented Double Zeta ANO for Cr). ELF values at attractors (η), basin populations ($N(\Omega_i)$), standard deviations ($\sigma^2(\Omega_i)$), relative fluctuations ($\lambda_F(\Omega_i)$), and contributions of the other basins (%) to $\sigma^2(\Omega_i)$, obtained for the $Cr(CO)_6$.

Ω	η	$N(\Omega_i)$	$\sigma^2(\Omega_i)$	$\lambda_F(\Omega_i)$	Contribution analysis (>10%)
C(C)	1.00	2.08	0.24	11.54%	38% V(Cr,C), 38% V(C, O), 13% V(O)
C(O)	1.00	2.14	0.34	15.89%	32% V(C,O), 61% V(O)
C(Cr)	1.00	21.30	2.47	11.60%	13% V(Cr,C)
V(O)	0.92	4.34	1.42	32.72%	15% V(Cr,C), 63% V(C, O), 14% C(O)
V(C,O)	0.86	3.12	1.45	46.47%	21% V(Cr,C), 61% V(O)
V(Cr,C)	0.93	2.76	1.30	47.10%	23% V(C,O), 25% C(Cr), 16% V(O)

delocalized towards oxygen (23% V(C,O) and 16% V(O)) as well as towards the chromium (C(Cr) weight amounts 25%) and the other V(Cr,C′) basins (20% total, 5% from each closer basin). The large distance between C(Cr) and V(Cr,C) (see Fig. 1 for the empty space between basins) suggests a closed-shell interaction with some correlation between Cr and C according to contribution analysis value for C(Cr) vs. V(Cr,C) and vice versa. There is a small disagreement between the number of electrons localized in Cr comparing ELF and QTAIM: while localization index of Cr was ca. 20 e, here we see the localized core basin locates 21.30 e. Taking into account, however, that these electrons are partially delocalized over V(Cr,C) basins, this disagreement can be considered minor and overall we may conclude QTAIM and ELF give a similar electron delocalization picture.

3.5. Mesomeric structures

The data provided by the topological analysis can be used to construct models which help the elucidation of the chemical bonding, namely, the phenomenological description of the chemical bonding in terms of superposition of mesomeric structures. Silvi proposes to make the following assessments [126]:

1. Electrons of the valence shell of an atom are distributed among the valence basins of such atom.
2. Monosynaptic basins carry nonbonding electrons (e.g. lone pairs, core electrons).
3. Polysynaptic basins contain bonding electrons between the basins connected.
4. Several electron pairs may be assigned to one given basin.

In order to illustrate this approach, we will follow Silvi and coworkers [127], and use the N_2 molecule as an example. N_2 molecule has a very simply topological structure with two core basins which contain the inner core electrons $1s^2$, C(N) and C(N′), two valence monosynaptic basins, V(N) and V(N′), corresponding to the lone pairs, and one bonding disynaptic basin, V(N,N′). We consider the following four mesomeric structures for N_2 molecule:

$$\underset{1}{\langle N=N|} \quad \underset{2}{|N=N\rangle} \quad \underset{3}{\langle N\text{–}N\rangle} \quad \underset{4}{|N\equiv N|}, \tag{27}$$

where "⟨" represents a couple of lone pairs. One may write a matrix which contains the expected number of electrons of the valence basins for each mesomeric structure:

$$\begin{array}{c|cccc} & \mathbf{1} & \mathbf{2} & \mathbf{3} & \mathbf{4} \\ V(N,N') & 4 & 4 & 2 & 6 \\ V(N) & 4 & 2 & 4 & 2 \\ V(N') & 2 & 4 & 4 & 2 \end{array} \cdot \begin{pmatrix} w_1 \\ w_2 \\ w_3 \\ w_4 \end{pmatrix} = \begin{pmatrix} N(V(N,N')) = 3.44 \\ N(V(N)) = 3.28 \\ N(V(N')) = 3.28 \end{pmatrix}. \tag{28}$$

And then calculate which would be the corresponding weight, w_i, for each structure so that the current population of each basin is fulfilled. This procedure yields $w_1 = w_2 = 0.31$, $w_3 = 0.33$ and $w_4 = 0.05$ at the B3LYP/6-311+G(2d) level. Although the value of the last mesomeric structure may seem surprising, in the ELF framework the contribution of p orbitals to the bonding basins and the V(N) is equally shared [127].

Let us now try to rationalize $Cr(CO)_6$ bonding from mesomeric structures. We propose three electron distributions:

$$\underset{1}{Cr\text{–}C=O>} \quad \underset{2}{Cr=C=O|} \quad \underset{3}{Cr-C\equiv O|}, \tag{29}$$

which generate the following set of equations to solve:

$$\begin{array}{c|ccc} & \mathbf{1} & \mathbf{2} & \mathbf{3} \\ V(O) & 4 & 2 & 2 \\ V(C,O) & 4 & 4 & 6 \\ V(Cr,C) & 2 & 4 & 2 \end{array} \cdot \begin{pmatrix} w_1 \\ w_2 \\ w_3 \end{pmatrix} = \begin{pmatrix} N(V(O)) = 4.34 \\ N(V(C,O)) = 3.12 \\ N(V(Cr,C)) = 2.76 \end{pmatrix}, \tag{30}$$

with solution $w_1 = 1.15$, $w_2 = 0.36$ and $w_3 = -0.48$. Among the configurations proposed the one that better fits the actual values of the basin population is **1**, which attributes some interaction to Cr–C pair and a highly polarized situation. This analysis, however, does not take into account the actual location of the basins involved. In the present case, one should mention that V(Cr,C) attractor is separated from C(Cr) attractor by 2.5 Å, while the distance between V(Cr,C) attractor and C(C) amounts only 1.1 Å; one can easily check it by examining Fig. 1. In addition, one may here compare this distance with the QTAIM atomic basin limits. The Cr–C BCP, which separates Cr and C atomic basins, lies 1.79 Å far from Cr attractor. Thus, most V(Cr,C) basin lies inside the carbon atomic basin further supporting a closed-shell dative type interaction. Since V(Cr,C) lies much closer to carbon than to chromium this mesomeric analysis in Eq. (30) is rather unrealistic. V(Cr,C) is actually much likely to be defined as V(C), and thus configurations in Eq. (29) do not represent the real distribution in the molecule according to ELF topology. Therefore, we have not pushed further the analysis of the mesomeric structures for this system. However, in general, to better reproduce the features of electron localization in the latter analysis one should include information regarding the second order density matrix.

In this sense, Silvi suggested a much more complete method of determining the weights of the molecular structures by also including information regarding the covariance of the electron population basins. In this case, apart from the Eq. (28) or Eq. (30) we would also include the covariance, leading to a set of equations for which the best values, in a least square sense, should be determined. See Ref. [126] for further details.

In order to carry out an ELF study of a given molecular system we recommend the ToPMoD package, which provides a suite of programs to perform all the analyses mentioned in this section [128]. Such a program can also perform a QTAIM analysis, and is thus worth considering for joint ELF-QTAIM studies.

4. Selected examples

We will start this section by analyzing the metal–ligand bonding in a series of complexes, leaving the special TM–carbonyl bonding for the next subsection. Section 4.3 is devoted to the TM–TM bonding, and Section 4.4 is left for the multicenter bonding in TM chemistry.

4.1. Metal–ligand bonding

The study of the molecular structure and bonding of TM complexes by means of DIs has been the subject of several studies. Let us start the discussion from the simplest species having just a metal and a ligand. So, the first work that we comment here refers to the study [129] of the ground and low-lying states of the simple doublet $Cu(H_2O)^{2+}$ species, an open-shell TM complex. The authors found that at the CCSD(T) level Cu^{2+}–H_2O presents C_{2v} symmetry and the ground electronic state is a $^2A_1$ state. At this level of theory the relative order of the electronic states is $^2A_1 < {}^2B_1 < {}^2B_2 < {}^2A_2$. On the other hand, DFT results show that the relative stability of these states vary depending on the degree of mixing of exact HF and DFT exchange functional. For pure and hybrid functionals with low percentages of HF mixing (up to 20–25%), the $^2B_1$ state becomes more stable than the $^2A_1$ one. These changes are related to the electronic delocalization in the different electronic

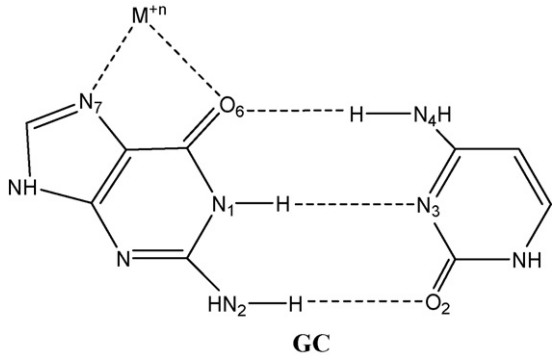

Fig. 3. Schematic representation of the cytosine-guanine base pair interacting with the metal cation. Taylor & Francis Ltd. http://www.informaworld.com, reprinted by permission of the publisher, Ref. [132].

states that was measured using DIs. For $^2B_1$, pure functionals provide a delocalized picture of the electron hole, whereas in the $^2A_1$ state the hole is more localized at the metal atom. Since delocalized situations are overstabilized by DFT functionals, the $^2B_1$ state is wrongly predicted to be lower in energy than the $^2A_1$ by pure functionals. The admixture of exact exchange in the B3LYP-like functionals reduces the error by reducing the degree of delocalization [130]. It was found that 40–50% mixing provides results in very good agreement with CCSD(T). More recently, the side-on (C_{2v}) and end-on (C_s) ground and lowest lying excited states of the doublet CuO_2 molecule have been examined with a similar procedure [131]. CCSD(T) results at the complete basis set limit showed that the relative stabilities of the different electronic states are $^2A_2(C_{2v}) < {}^2A''(C_s) < {}^2B_2(C_{2v}) < {}^2A'(C_s) \ll {}^2A_1(C_{2v}) < {}^2B_1(C_{2v})$. At variance with CCSD(T), all DFT methods analyzed in this work (including B3LYP-like methods incorporating different degrees of exact exchange) erroneously predict the end-on $^2A''$ state as the ground state for CuO_2 irrespective of the type of functional used. However, unlike $Cu(H_2O)^{2+}$, the overestimated stability of the end-on $^2A''$ state at the DFT level cannot be ascribed to differences in electronic delocalization between the end-on $^2A''$ and side-on $^2A_2$ states, since in both states the unpaired electron is almost totally localized on the Cu atom. Thus, the reason for the DFT computed higher stability of the $^2A''$ relative to $^2A_2$ state was ascribed to the larger covalent character of the former state.

In a subsequent work [132], the DIs were use to analyze how metal cations (M = Cu^+, Ca^{2+}, and Cu^{2+}) coordinated to the N_7 of guanine (see Fig. 3) and ionization affect the nature of the hydrogen bonds (H-bonds) and the aromaticity of the different rings for the Watson–Crick guanine-cytosine base pair (GC) [132]. Table 4 contains the B3LYP aromaticity results (for the indices used, we have that the more negative the NICS [133], the lower the FLU index [92], and the higher the HOMA [134] and PDI values [91], the more aromatic are the rings) for the 6- and 5-MRs studied (see Fig. 3). The H-bond formation in GC implies a certain loss of π-charge in N_1 and a gain in O_6, respectively, thus increasing the relevance of the resonance structure **2** (see Fig. 4), which favors the intensification of the aromatic character of the guanine 6-MR. The increase of the aromaticity of the guanine and cytosine 6-MRs due to the interactions with Cu^+ and Ca^{2+} is also attributed to the strengthening of H-bonding in the GC pair, which stabilizes the charge separation resonance structure **2** [135,136]. This effect is stronger for the divalent Ca^{2+} metal cation than for the monovalent Cu^+. Meanwhile, the observed reduction of aromaticity in the 5- and 6-MRs of guanine due to ionization or the interaction with Cu^{2+} is caused by the oxidation process that removes one π-electron, disrupting the π-electron distribution. In a recent related work, the influence of metal cations (Na^+, K^+, Mg^{2+}, and Ca^{2+}) on the aromaticity of the six-membered rings of phenylalanine and tyrosine has been discussed in terms of multicenter bond indices [137]. The results show that interaction of the metal cations with the aromatic ring of the amino acids reduces the aromaticity of the complexed species as compared to the isolated states. The effect is larger for the divalent cations.

Let us now consider the TM complexes with multiple ligands. The bonding to titanium has been studied in two studies by means of DIs. For the hypovalent titanium alkoxide model complexes, Dobado et al. [138] found that the values of δ(Ti,O) ranging from 0.96 to 1.08 e were consistent with a Ti–O polarized triple bond with significant covalent character. The ELF analysis revealed a spherical monosynaptic basin, V(O), with a population of roughly six electrons pointing towards the C(Ti) basin, corresponding to Ti–O bonding and indicative of triple bonding highly polarized (the bonding basin is exclusively attributed to Ti). This is corroborated by the observation that C(Ti) and V(O) are highly correlated. On the other hand, Bader and Matta [139] analyzed the nature of Ti–C contacts in a Ti bonded to cyclopentadienyl and a substituted dienyl complex to determine whether these interactions should be considered as short nonbonded contacts or agostic interactions. The low DIs found by these authors and the lack of Ti–C bond paths were consistent with the former hypothesis.

In another study, the bonding in a series of 25 Fischer carbene complexes of the type $(CO)_5Cr{=}C(X)R$ (X = H, OH, OCH_3, NH_2, $NHCH_3$ and R = H, CH_3, $CH{=}CH_2$, Ph, C≡CH) was analyzed using DIs [140]. The electron delocalization between the Cr and C atoms (that ranges from 0.623 to 1.124 e) and between the C atom and the X group (from 0.931 to 1.332 e), both typical of single bonds, are related to the π-donor strength of the X group and the degree of backdonation between the chromium pentacarbonyl and the carbene fragments. Thus, for a given R, δ(Cr,C) decreases in the order $H > OH > OCH_3 > NH_2 > NHCH_3$, while the increase of the π-donor character follows the opposite order. The increase in the π-donor character of the X substituent partially switches off the backdonation mechanism and this is reflected in the reduction of the δ(Cr,C) values. Small negative values of the 3-center DIs [141–145] (Eq. (12)) between Cr, C, and X and the significant δ(Cr,X) values were

Table 4
NICS (ppm), PDI (electron pairs), HOMA, and FLU aromaticity measures of the five- and six-membered rings of guanine (G) and six-membered ring of cytosine (C) computed with the B3LYP method.[a]

System	NICS			PDI		HOMA			FLU		
	G-5	G-6	C-6	G-6	C-6	G-5	G-6	C-6	G-5	G-6	C-6
GC	−11.94	−4.10	−1.86	0.036	0.040	0.848	0.795	0.703	0.025	0.033	0.035
$[GC]^{\bullet+}$	−5.41	−0.31	−2.49	0.023	0.042	0.829	0.550	0.773	0.028	0.048	0.031
Ca^{2+}–GC	−10.67	−4.76	−2.53	0.044	0.045	0.843	0.886	0.797	0.023	0.024	0.029
Cu^+–GC	−10.64	−4.59	−2.25	0.040	0.043	0.869	0.898	0.761	0.021	0.027	0.032
Cu^{2+}–GC	−7.37	−2.00	−3.07	0.022	0.040	0.915	0.760	0.822	0.033	0.058	0.039

[a] Taylor & Francis Ltd. http://www.informaworld.com, reprinted by permission of the publisher, Ref. [132].

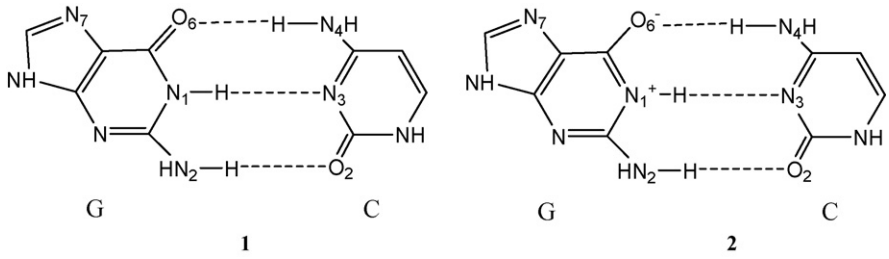

Fig. 4. Schematic representation of the charge transfer in GC base pair. G refers to guanine, whereas C to cytosine. Taylor & Francis Ltd. http://www.informaworld.com, reprinted by permission of the publisher, Ref. [132].

consistent with the hypothesis of a weak three-center four-electron (3c-4e) bonding interaction in the Cr = C–X group of atoms.

4.2. Bonding in M–CO species

The bonding between TM atoms and CO is of vital importance to understand molecular chemistry and surface chemistry. A typical description of M–CO bonding uses the model of Dewar, Chatt and Duncanson (DCD) [72,73], namely, σ donation from CO to the empty orbital of the TM and π-backdonation from the TM to the CO π^* orbital (see Fig. 5). This π-backdonation correlates with the C–O bond distance.

We will first concentrate on the bonding between first-row TM and carbonyl ligands in monocarbonyl M–CO species, as analyzed by Pilme et al. [146]. QTAIM charges show significant electron transfer from the TM to the carbonyl, the Laplacian of the electron density at the BCP of M–C bond is large and positive, indicative of charge depletion in the M–C bond. The values of the DI for M–C are also quite large, an indication of significant electron delocalization between the TM and the carbon atom. The values range 0.84–1.76 e, and represent a closed-shell interaction involving a charge transfer, as indicated by the positive charges of the TM. Thus according to QTAIM the M–C bonding can be classified as dative. Taking a look at the spin population (see Eq. (26)), QTAIM enables the classification of compounds in high spin, low-spin, and conserved spin multiplicity complexes. High spin complexes are characterized by large electron transfer and their DI show an intermediate value (ca. 1.2 e), low spin complexes exhibit small charge transfer but have large δ(M,C) (ca. 1.6 e), while conserved spin multiplicity complexes display both small charge transfer and δ(M,C).

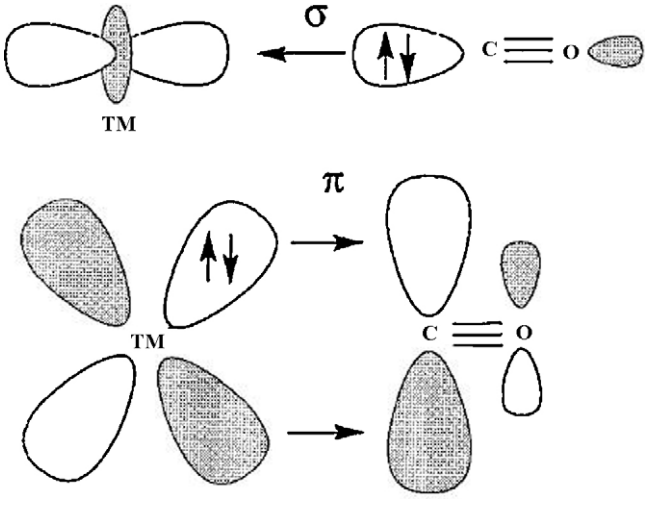

Fig. 5. Schematic representation of the synergistic OC → TM σ-donation and OC ← TM π-backdonation. An example of the Dewar–Chatt–Duncanson model. (Reproduced with permission from Ref. [15]. Copyright 2000 American Chemical Society.)

ELF analysis exhibits different results for linear and bent monocarbonyl systems. The first noticeable difference is the bifurcation point at which V(M) and C(M) separate from the main localization domain. For linear molecules the basin associated with the lone pair, V(M) separates first in the bifurcation diagram, leaving C(M) in the same localization domain than V(M,C). According to Silvi and coworkers [146] this is an indication that here the 3d subshell has an ambivalent character, sharing both core and valence basin of the TM. On the other hand, bent molecules show a bifurcation diagram where C(M) separates first than V(M), indicative of the lesser valence character of subshell 3d for these molecules as compared to the linear ones.

The ELF also allows for the proposal of an occupation scheme based on the weighting assigned to a set of configurations, using a technique analogous to that explained to obtain the weights of different mesomeric forms. In this way, Pilme et al. [146] investigated the occupancy of C(M), *c*, V(M), *v*, and the charge transferred, *l*, by using a set of configurations consistent with the spin multiplicity. Interestingly, for complexes whose TM bears atomic number $Z = 20 + n$ the spin multiplicity is given by Hund's rule for the configuration $[Ar]c^{n+2}$, excepting for Cr, Mn, and Cu complexes. $[Ar]c^{n+2}$, $[Ar]c^{n+1}v^1$, $[Ar]c^{n+1}l^1$, $[Ar]c^{n}l^2$, and $[Ar]c^{n-1}v^1l^2$ are the configurations possible for high-spin complexes. The authors observed how the weight of $[Ar]c^{n+2}$ increases with *Z*, whereas $[Ar]c^{n-1}v^1l^2$ decreases for the series TM = Sc, Ti, and *V*, thus leading to higher charge transfer. Low-spin complexes in the series TM = Fe, Co, Ni, have three configurations, $[Ar]c^{n+2}$, $[Ar]c^{n}v^2$, and $[Ar]c^{n-2}l^4$ and also show how $[Ar]c^{n+2}$ increases with *Z*, but at the expense of $[Ar]c^{n}v^2$, leaving $[Ar]c^{n-2}l^4$ constant and thus the charge transfer.

A common feature of both linear and bent systems is the nature of the C–O entity, which appears to be a well-defined chemical subunit. For all systems the last separation in the bifurcation diagram occurs for C–O, as the localization domain of V(O) absorbs the basin corresponding to the bonding region V(C,O). This an indication of the strong polarization of C–O bond, due to the difference of electronegativities. One can calculate the charge transfer from the TM to the CO unit, by summing the populations of the valence and the core basins of the metal and extracting it from the atomic number. For high-spin complexes there is a decrease of the net charge transfer with increase of TM atomic number, consistent with the chemical intuition of smaller charge transfer with higher electronegativity of the TM.

Interestingly, for high-spin complexes, the population of V(C,O) basin correlates very well with the C–O bond length. In this sense, since C–O bond length also correlates with π-backdonation, it is reasonable to believe that this effect should be reflected in V(C,O) population. However, Pilme et al. [146] estimated the topological donation and backdonation by other means. For the QTAIM, they calculated the contribution of the σ orbitals from the carbon and the oxygen basins, and subtracted the total occupation of these

Table 5
B3LYP/(6-311+G(2d) for C, O and TZV for the TM) QTAIM and ELF donation and backdonation for linear MCO complexes (M = Sc, Ti, V, Fe, Co, Ni). From Ref. [146]. All quantities are given in a.u.

	σ donation		π backdonation	
	QTAIM	ELF	QTAIM	ELF
ScCO	0.14	−0.03	0.78	1.05
TiCO	0.17	0.02	0.69	0.87
VCO	0.21	0.08	0.64	0.82
FeCO	0.42	−0.02	0.68	1.08
CoCO	0.41	0.0	0.67	1.09
NiCO	0.41	0.06	0.68	1.06

orbitals to provide an estimate of σ-donation. The sum of the contribution of π valence orbitals to the metal basin with respect to the total occupation of these orbitals gave likewise an estimate of π-backdonation. The same reasoning can be followed for the ELF partition, with the exception that the occurrence of V(C,M) is attributed entirely to the ligand in agreement with the previous observation that there is a reducible localization domain which contains only V(C,M) and the C–O fragment. Table 5 summarizes the results for the linear complexes taken into study.

One can immediately see that ELF yields negligible σ-donation and π-backdonation close to 1 electron, while QTAIM donation is noticeable larger (especially for high-spin complexes which carry ca. 0.4 electrons donation) and backdonation of ca. 0.7 electrons. In a sense, ELF approach support a scheme very close to $M^+(CO)^-$, whereas QTAIM yields an scheme which also resembles $M^+(CO)^-$ for low-spin complexes but differs slightly for high-spin complexes. Both approaches, QTAIM and ELF attribute more importance to the backdonation rather than to the donation in carbonyl complexes, as do most other studies to date [15].

The bonding in TM carbonyl complexes has also been examined using DIs in other studies. Macchi et al. [46,147,148] analyzed the series of TM carbonyl complexes given in Table 6. They found the expected decrease of the δ(C,O) values in TM carbonyl complexes as compared to free CO due to a weakening of the C–O bonding when the carbonyl is coordinated to the TM following DCD scheme. They considered that the most reasonable sign of the backdonation mechanism comes from the δ(M,O) values which are relatively large (from 0.09 to 0.22 e) compared to the H_3BCO species (0.04 e) in which a classical donor–acceptor bond is found and the backdonation mechanism is inoperative. The reason is that σ-donation involves mainly metal and carbon orbitals, while in π-backdonation the contribution coming from oxygen orbitals is significant. Cortés-Guzman and Bader [99] analyzed the same series of TMs, except for the $[(CO)_3Co–CO]^-$, $[(CO)_3Ni–CO]$, and $[(CO)_3Cu–CO]^+$ species, reaching similar conclusions. These authors emphasized the significant degree of delocalization between the metal and the carbon atoms, with δ(M,C) values close to unity, which points to an equal sharing of an electron pair between the metal and each of the C atoms. The amount of electronic charge from the metal that is delocalized onto the remaining atoms, $\delta(M)$, is 2.9, 3.0, and 2.3 e for $Cr(CO)_6$, $Fe(CO)_5$, and $Ni(CO)_4$, respectively. The electron localization in the carbon atom changes from 81% in free CO to about 70% in the complexes, in line with the bonding mechanism just mentioned. In the same work, Cortés-Guzman and Bader analyzed the bonding in ferrocene, $Fe(Cp)_2$. The δ(Fe,C) value is 0.45 e, i.e., about 2.25 e shared between the cyclopentadienly ring and the Fe atom. The number of electrons of the metal that are delocalized onto the remaining atoms is 2.4 compared to 3.0 for $Fe(CO)_5$, which is consistent with two electron pairs interacting between the metal and the ring.

Table 6
B3LYP delocalization indices $\delta(A,B)$ (in electrons) for some transition metal carbonyl complexes[a].

Molecule	δ(C,O)	δ(M,C)	δ(M,O)
CO	1.80		
H_3BCO	1.65	0.50	0.04
$(CO)_5Cr–CO$	1.62	0.83	0.14
$(CO)_4Fe–CO_{eq}$	1.61	1.05	0.18
$(CO)_4Fe–CO_{ax}$	1.61	0.98	0.17
$[(CO)_3Co–CO]^-$	1.53	1.23	0.22
$(CO)_3Ni–CO$	1.66	0.98	0.16
$[(CO)Cu–CO]^+$	1.82	0.74	0.09

[a] From Ref. [46].

Macchi and Sironi [148] have recently analyzed the previous series of TM complexes by substituting one or two CO groups by ethene to give the $(CO)_5Cr(C_2H_4)$, $(CO)_2Ni(C_2H_4)$, and $(CO)_4Fe(C_2H_4)$ complexes. The δ(C,C) values in these complexes are 1.52, 1.42, and 1.33 e. The lower the δ(C,C) values, the higher the degree of C–C bond activation in the different complexes. Similar results are reported by the same authors for the $(CO)_5Cr(H_2)$ and $(PH_3)_5Cr(H_2)$ species. In these systems, the δ(H,H) values are 0.70 and 0.61, respectively, thus indicating a higher activation in the case of the $(PH_3)_5Cr(H_2)$ complex.

Studies into the bonding of first-row TM with other ligands such as the π-acceptors N_2, C_2H_2, CN^-, and the σ-donors NH_3, H_2O and F^- have been reported [127]. The neutral acceptor ligands behave in a manner very similar to CO, already described at the beginning of this section. On the other hand, CN^- behaves in a quite different way, similarly to σ-donor ligands. In these complexes the metal is polarized by the electron transfer observed between the core, $C(M)$, and the valence, $V(M)$ basins. This fact is further supported by the observation that $[Ar]c^n$ core configuration determines the spin multiplicity.

4.3. Metal–metal bonding

First-row TMs were extensively covered in the last section because of their ability to form TM–carbonyl compounds, and some first-row TMs also contribute to polynuclear TM–carbonyl compounds. However, heavier TMs are more prone to form strong TM–TM bonds. Namely, TM–TM bonding is usually given between elements of the second and the third transition series [149]. TM carbonyl compounds contain TM in low oxidation states, and it is thus not surprising to find among them several species containing TM–TM bonds. Most of these species exhibit a simple bond pattern, with a pair of electrons holding the TM–TM bond, and both TM attaining an 18-electron configuration (*vida supra* for 18-electron rule).

The bonding between TMs becomes trickier as polarity comes into play. The different nature of the ligands attached to the TMs or the linking of different TM (giving rise to heterobimetallic complexes) leads to a certain degree of TM–TM bond polarity. A way to generate highly polar TM–TM bonds is by combination of complex fragments from extremes of the d-block periodic table [150]. The idea behind is to bond d-electron rich metal centers with d-poor metal ones, in what are known as “early–late” heterobimetallic complexes, in reference to early TM and late TM constituting the TM–TM bond.

Usually bond polarity is recognized by different partial *atomic* charges. This practice is somewhat controversial since different atomic charges may give quite different values for the same compound [71], as commented in Section 1. In this respect, although QTAIM atomic charges have been taken as measures bond polarity, results have to be analyzed with caution. For this reason, it is desirable to use other descriptors less dependent on the particular approach studied. Bond orders (or more generally ESI) have been

repeatedly proven in the literature to be less basis-set and method dependent than partial charges. The QTAIM-ESI (or simply DI) can be calculated in the TM–TM bonds, as well as in the bonds involved in the ligand to assess the effect of the polarization.

The $(H_2N)_3Ti–Co(CO)_4$ and $(H_2N)_3Ti–Co(CO)_3(PH_3)$ bimetallic complexes were analyzed by means of QTAIM atomic charges and DIs at the B3LYP/TZP level in TM complexes by Jasen et al. [151]. $(H_2N)_3Ti–Co(CO)_4$ reported a charge of 1.99 e over titanium, and 0.30 e over the cobalt atom. The Ti–Co DI was shown to be 0.42 e, quite below the values expected in a regular covalent bond, giving support to a strongly polarized bond. Similarly for $(H_2N)_3Ti–Co(CO)_3(PH_3)$ one finds a TM–TM polarized situation where Ti and Co QTAIM atomic charges are 1.99 and 0.18 e, respectively, while Ti–CO DI is 0.42 e. One may also observe the effect on the neighboring bonds. For instance, in both complexes C–O DI values drop about 0.3 units with respect to the value given in the free molecule, while C–Co ESI was slightly greater than 1 e, reflecting the polarization given by the TM–TM pair. However, the value of the TM–TM DI (quite below 0.5 e) for both complexes may suggest that the interaction between TMs is ionic rather than covalent. In order to assess this point, one might take a look at the value of the density at the BCP between TMs, the Laplacian of the density in the vicinity of the BCP and the energy density. However, these results give some ambiguity on the character of the bond: on one hand the density at the BCP is ca. 0.05 a.u., typical of closed-shell interaction (supporting thus ionic TM–TM bond) and the Laplacian is ca. 0.04 a.u., a positive value which indicates small electron depletion, on the other hand, the value of the energy density is ca. −0.012 a.u. which is a typical value for covalent interactions. With this scenario the authors [151] decided to study the ELF for these systems providing room for the interpretation of bond polarity by other means.

The ELF locates a bonding basin between TMs (see Fig. 6), with a maximum value of 0.46, a quite low value compared to the typical values of covalent molecules. This explains why the ESI value was so small: there is indeed some electron charge delocalized between both TMs, but it is quite small to fully consider a covalent bond. The authors argue that this low ELF value is due to the low participation of d-orbitals in the bonding. However, as already demonstrated by Kohout et al. [152] the lowering of the ELF values is achieved only when d-orbitals are uniformly occupied. Following the reasoning of this latter work one is tempted to believe the situation is similar to that given in $Re_2(CO)_{10}$, where the bonding basin between rhenium atoms was originated from the interaction between the core and valence electrons.

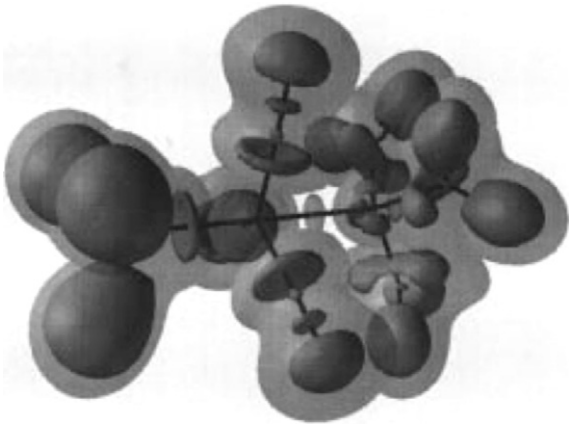

Fig. 6. ELF = 0.42 and ELF = 0.83 isosurfaces superimposed for $(H_2N)_3Ti–Co(CO)_3(PH_3)$. The molecule is depicted with $\{(PH_3)(CO)_3Co\}$ unit in the l.h.s. and with $\{Ti(H_2N)_3\}$ unit on the r.h.s. (Reproduced with permission from Ref. [151] Copyright 1998 American Chemical Society.)

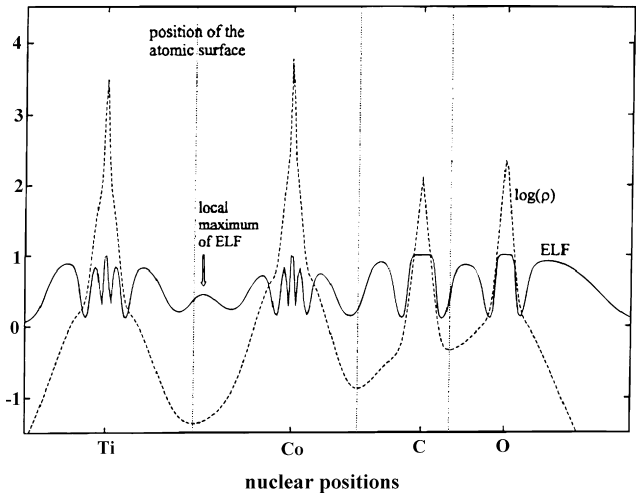

Fig. 7. Density (dashed line) and ELF (solid line) profiles for $(H_2N)_3Ti–Co(CO)_4$. The QTAIM atomic boundaries are indicated as vertical dotted lines. (Reproduced with permission from Ref. [151]. Copyright 1998 American Chemical Society.)

Further inspection of the ELF picture reveals strong polarization of Ti–N bond toward the N atom. A nice way to combine QTAIM and ELF approaches consists of the simultaneous plotting of both functions, so that one may see in which atomic basin lies each bonding basin. In this case, one may observe how all ELF isosurfaces around the ligands do not cross the QTAIM atomic separating surfaces. In addition, the TM–TM bonding basin is essentially concentrated in the Co atomic basin. This gives further support to the TM–TM bond polarization, and explains why both the density and the Laplacian of the density at the BCP (lying in the separating surfaces) showed low values (see Fig. 7).

The nature of metal–metal bonding in organometallic species and clusters has been analyzed using DIs in several studies. In one of the first, Yu and Dolg [153] reported that the DIs for the dimers Zn_2, Cd_2, and Hg_2 are 0.14, 0.19, and 0.19 e, respectively, at the CASSCF level. In comparison to those found for Cu_2, Ag_2, and Au_2 of about 0.62 e, the authors concluded that the DIs in Zn_2, Cd_2, and Hg_2 are between those of typical van der Waals complexes and covalent single bonds. So, the bonding in the group 12 dimers can be viewed as mixture of (3/4) van der Waals and (1/4) covalent interaction. The metal–metal bond in Mo_2 and V_2 molecules was studied by Ponec, Yuzhakov, and Carbó-Dorca at the B3LYP level using the DAFH associated with a single atom in the diatomic molecule [68]. The analysis of the DAFH is carried out through the diagonalization of the matrix that represents the hole in the basis of atomic orbitals (AOs). Then, the number of obtained eigenvalues close to one in the diagonalization process is an indication of the bond order. From their results, the authors concluded that the bond order in the Mo_2 and V_2 molecules is four and five, respectively.

The most studied metal–metal bonds are, however, those present in homoleptic $M_m(CO)_n$ dimers or trimers ($m = 2$ and 3). The D_{3d} $Co_2(CO)_8$ and $[FeCo(CO)_8]^-$ complexes (species **1** and **2** in Fig. 8) were analyzed by Macchi et al. [147,148] to discuss the possible existence and nature of metal–metal bonding. For the $Co_2(CO)_8$ species [148], the δ(Co,Co) is 0.46 e, which is significantly smaller than the value of 1.0 expected for an electron pair sharing corresponding to a two-center two-electron bonding (2c-2e). According to the authors, this is due to the weak 1,3-interactions that take place between the metal and all the vicinal carbonyls. Indeed, the δ(Co,C) is as large as 0.07 e. Thus, if one sums the δ(Co,Co) and all δ(Co,C) contributions, the electron pair sharing formally associated with a single Co–Co bond of about 1.0 e is recovered. This

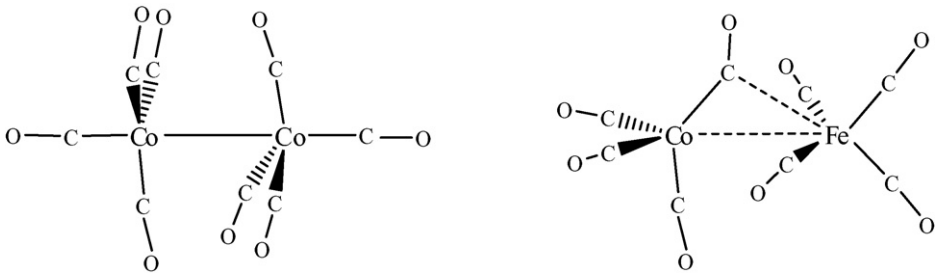

Fig. 8. An schematic representation of the D_{3d} $Co_2(CO)_8$ and $[FeCo(CO)_8]^-$ complexes.

is an important result that shows that the bonding metal–metal electron pair is quite delocalized and a fully localized 2c-2e bond does not exist. As can be seen in Fig. 8, there is a semi-bridging carbonyl group in $[FeCo(CO)_8]^-$. The same authors analyzed the hypothetical transformation of a carbonyl from terminal to symmetrically bridging in $[FeCo(CO)_8]^-$ by means of DIs [147]. During this terminal to bridge conversion, there is a change from a formally 2c-2e Co–CO bond to a 3c-4e bond in Co–CO–Fe. This change is followed by a smooth decay of the δ(Fe,Co), which has an almost constant value of 0.4 e, and an increase of the δ(Fe,C) and a decrease of the δ(Co,C) values for the bridging carbonyl group, the rest of the DIs being approximately constant. Thus the DIs of the Fe–Co and M–C interactions remain almost constant along the interconversion path. This is in line with the observed carbonyl fluxionality in this kind of TM complex. Thus, for all systems along the reaction path the Fe–CO–Co bonding is characterized by the presence of direct Fe–Co and indirect M–C interactions that result in substantial and constant delocalization through the hypothetical transformation. The results show that even in the absence of M–M bond paths, there is a considerable metal–metal delocalization indicative of M–M bonding. In addition, the significant δ(Fe,O) and δ(Co,O) values are in line with substantial π-backdonation. More recently, Farrugia [154] studied the Co–Co bonding in $Co_2(CO)_6(\mu\text{-}CO)(\mu\text{-}C_4H_2O_2)$ reaching the conclusion that the δ(Co,Co) value in this complex is similar to that of $Co_2(CO)_8$ in its bridged form, but somewhat smaller than for the unbridged form **1**. This was interpreted considering that the sharing of electrons between Co centers can occur via bridging interactions. Very recently, Ponec et al. have discussed the bond in $Fe_2(CO)_9$ and $Co_2(CO)_8$ by means of domain averaged Fermi holes [70]. Their analysis shows that there is no direct metal–metal bond in these species. The authors also found the existence of delocalized multicenter bonding electron pairs, which is not surprising because there are not enough electron pairs in these complexes to form localized 2c-2e bonds. Finally, Chevreau et al. [155] analyzed the nature of the chemical bonding in the D_{3h} and C_{2v} isomers of $Fe_3(CO)_{12}$. They found that the DIs are rather small for Fe–Fe interactions (~0.4 e, closed shell interaction), of the order of 1 e for the Fe–C dative bond, and of 1.6 e for C–O. In line with the results discussed in the last section, these authors found that π-backdonation decreases the δ(C,O) values in TM carbonyl complexes by about 0.2 e with respect to free CO. In the same work the analysis of the ELF showed V(C,O) basin populations 0.12–0.46 e smaller than that found in free CO. Global ELF populations were also shown to agree with a $[Ar]d^6$ configuration.

The $[(Cr_2(\mu_2\text{-}H)(CO)_{10}]^-$ complex was also the subject of an interesting study using DIs to discuss the nature of the Cr–H–Cr bond [148,156]. Three conformers of similar energy can be located in the potential energy surface of this complex. In the conformer with D_{4d} symmetry, the Cr–H–Cr bond is linear, while in the C_2 and C_s conformers it is bent. In the most stable C_s (and also in the D_{4d}) conformer the carbonyl groups in one $Cr(CO)_5$ moiety are staggered with respect to carbonyls in the other. As can be seen in Table 7, the Cr–H delocalization in the $[(Cr_2(\mu_2\text{-}H)(CO)_{10}]^-$ complex is slightly larger than one half of the value for $[(Cr(CO)_5H]^-$. This result together with the significant δ(Cr,Cr) value is consistent with the presence of a 3c-2e bond similar to that found in borane (see Table 7). In the bent C_s conformer, the metal–metal delocalization is only slightly larger than that found for the D_{4h} isomer (the D_{4h} conformer is the same as the D_{4d} but with the carbonyls eclipsed), suggesting that a possible direct metal–metal bond is not present in the C_s species. Also remarkable is the significant delocalization of 0.08 and 0.05 e for the C_s and D_{4h} isomers, respectively, found between the H bridge and the *C* atom of the equatorial carbonyls. This result was confirmed from the picture of the Fermi hole density distribution. Strong similarities were found in the comparison between the results of the $[(CO)_5Cr\text{–}H\text{–}Cr(CO)_5]^-$ and $[(CO)_5Cr\text{–}H\text{–}BH_3]^-$, which is not totally unexpected given the fact BH_3 and $Cr(CO)_5$ are considered isolobal fragments. Although the differences increase when comparing the $[(CO)_5Cr\text{–}H\text{–}Cr(CO)_5]^-$ and $[(CO)_5Cr\text{–}H\text{–}CH_3]$ species, the bonding parameters are still quite similar. In the latter, there is a more asymmetric agostic interaction between methane and the $Cr(CO)_5$ group. The authors conclude that, although the agostic M···C–H and the symmetric hydride bridge M–H–M interactions lead to quite different geometries, they share the same bonding nature. In fact, one could speak of a symmetry-stabilized agostic interaction in the $[(Cr_2(\mu_2\text{-}H)(CO)_{10}]^-$ complex.

The metal–metal bonding of $M_2(CH_3)_6$ (M = Mo, W), $W_2Cl_8^{4-}$, and $Re_2Cl_8^{2-}$ has been studied by Ponec et al., in two papers, by means of DAFHs [68,157]. For the $M_2(CH_3)_6$ (M = Mo, W) species, the analysis confirmed the existence of a metal–metal triple bond involving one σ and two π components formed by combination of metal d orbitals of appropriate symmetry. For the $W_2Cl_8^{4-}$ complex, the diagonalization of the matrix that represents the hole in the basis of AOs yields four eigenvalues close to unity, i.e., a quadruple metal–metal bond. Analysis of the corresponding eigenvectors show one σ, two π, and one δ contributions to the total bonding. In the case of $Re_2Cl_8^{2-}$ the results showed that although the Re–Re

Table 7
BP86 bond distances (in Å) and delocalization indices $\delta(A,B)$ (in electrons) for the $[Cr_2(\mu_2\text{-}H)(CO)_{10}]^-$ complex and related species.[a].

Y–H–X	d(**Y–H**)	δ(**X–H**)	δ(**X,Y**)
$[(CO)_5$**Cr–H**$]^-$	1.650	0.59	–
D_{4h} $[(CO)_5$**Cr–H**–$Cr(CO)_5]^-$	1.767	0.38	0.07
C_s $[(CO)_5$**Cr–H**–$Cr(CO)_5]^-$	1.769	0.38	0.09
$[(CO)_5$**Cr–H**–$BH_3]^-$	1.752	0.38	0.07
$[(CO)_5$**Cr–H**–$CH_3]$	2.009	0.13	0.11
B_2H_6, $[H_2$**B–H$_2$**–$BH_2]^-$	1.321	0.37	0.12

[a] From Ref. [156].

bond involves four electron pairs, the bonding contribution of one of them is partially cancelled due to fractional occupation of the corresponding antibonding orbital [157].

4.4. Multicenter bonding

In this section, we will review some examples in the literature where TMs are involved in multicenter bonding. In order to identify and characterize this kind of bonds the ELF is a usual candidate of choice, however, multicenter indices (see Eqs. (12) and (13)) within the QTAIM or some other interesting partition, have also been used to characterize multicenter bonding. We will split the section into two parts, in the first we will review multicenter bonding in which TMs are not the only kind of atoms involved, whereas the second part will be devoted to multicenter bonding between TMs.

4.4.1. Involving TM and other atoms

The most paradigmatic example of multicenter bonding is perhaps the diborane molecule [158]. Due to the particular structure of boron, it is not surprising that metallaboranes are also prone to display multicenter bonding [159]. Particularly interesting is the structure recently synthesized by Braunschweig et al. [160], a metalloborylene where boron atom lies in the coordination sphere of three TMs, [η_5-(C_5Me_5)(OC)Fe(μ-CO)Pd(PCy_3)(μ-Br)Pt(PCy_3)Br(μ^3-B)] (see Fig. 9). These authors performed an ELF calculation of two simplified molecules, [η^5-(C_5H_5)(OC)$_2$Fe–B = $PtBr_2$–(PMe_3)] and the resulting molecule after the addition of the {Pd(PMe3)} moiety: [η^5-(C_5H_5)(OC)Fe(μ-CO)Pd(PMe_3)(μ-Br)Pt(PMe_3)Br(μ^3-B)]. The first molecule showed the presence of a ring attractor, which gives rise to a bonding basin, in a typical ring shape occurring for π-bonding between Pt and B atoms, as the authors suggested, pointing out triple bond character. Interestingly, the addition of the {Pd(PMe_3)} changes the picture: the ring attractor becomes a point attractor and the bonding basin becomes asymmetrical. The bonding basin of B–Fe now affects the palladium center, in a picture which could be described as a 3c-2e bonding (see Fig. 10). The authors do not provide more data to further characterize this bond. The synaptic order of the basins, as well as the covariance between the basins involved in the three-center bonding could have shed some light in the bonding situation, to completely assess the 3c-2e character of the bonding.

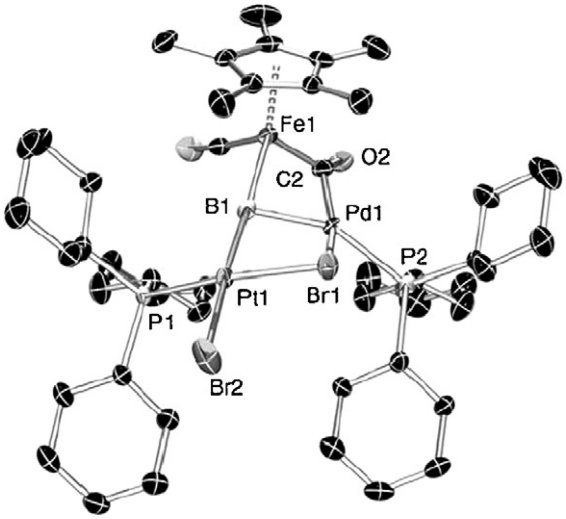

Fig. 9. Molecular structure of η^5-(C_5Me_5)(OC)Fe(μ-CO)Pd(PCy_3)(μ-Br)Pt(PCy_3)Br(μ^3-B). (Reproduced with permission from Ref. [160]. Copyright 2006 Wiley–VCH Verlag Gmbh & Co. KGaA, Wienheim.)

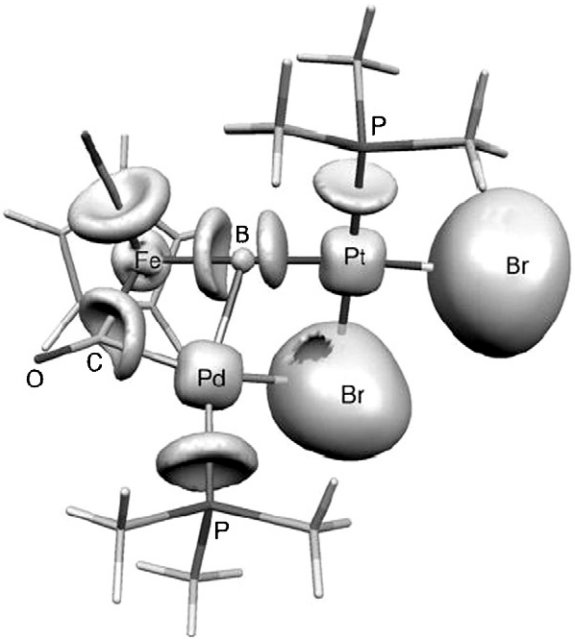

Fig. 10. ELF = 0.7 picture for the model complex η^5-(C_5H_5)(OC)Fe(μ-CO)Pd(PMe_3)(μ-Br)Pt(PMe_3)Br(μ^3-B). (Reproduced with permission from Ref. [160]. Copyright 2006 Wiley–VCH Verlag Gmbh & Co. KGaA, Wienheim.)

Another striking example of TM multicenter bonding is the case recently presented by Fowe et al. [161] where the authors pose two alternative representations for [(η^6-Arene)$_2$Ru$_2$(μ_2-H)$_3$]$^+$ complex, one with three-center bonds through bridging hydrogen atoms, and the other with a triple bond (see Fig. 11). The analysis of the topology of the density shows a bond path connecting Ru–Ru bonds through a BCP where the density attains a value of 0.016 a.u. and the Laplacian is negative, −0.078. In spite of the existence of a BCP, the value of the density and the Laplacian are quite low to represent a covalent interaction, and, as the authors suggest, the values are definitely too low to represent a multiple bond. Again, the study of the ELF sheds more light into the problem. Fig. 12 displays the ELF isosurfaces for two different values of the function. We can recognize three trisynaptic basins V(Ru, H, Ru) which immediately suggest a three-center bonding, further supported by the fact that there is no disynaptic bonding basin lying in Ru–Ru line which could be assigned to a Ru–Ru bonding. In addition, the population of the trisynaptic basin (1.8 e) is consistent with 3c-2e bonding. In the contour plot displayed in Fig. 12 one may also see at the Ru–Ru

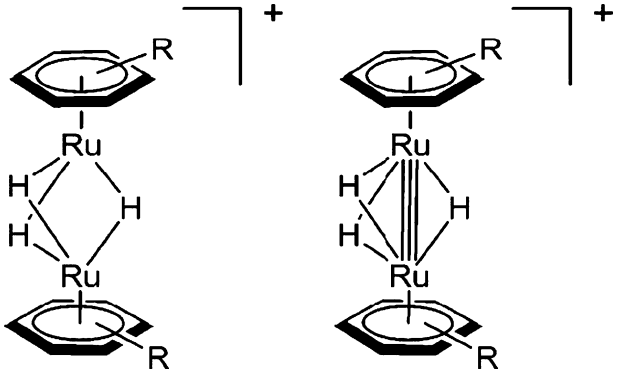

Fig. 11. Alternative representations of the electron-deficient complexes [(η^6-Arene)$_2$Ru$_2$(μ_2-H)$_3$]$^+$. (Reproduced with permission from Ref. [161]. Copyright 2008 American Chemistry Society.)

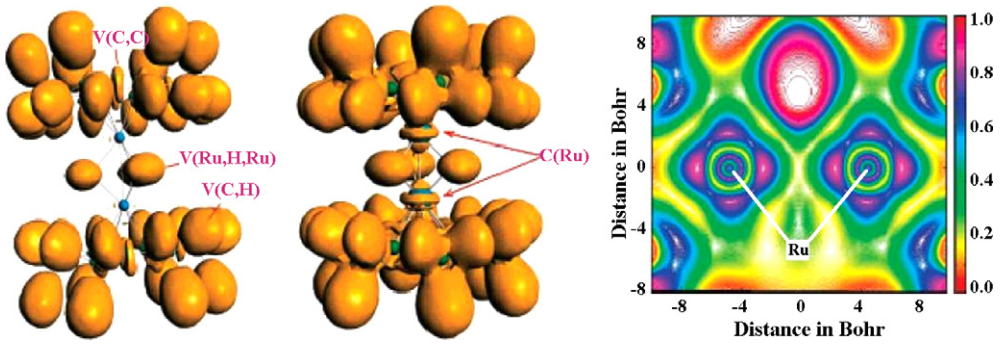

Fig. 12. ELF = 0.75 and ELF = 0.6 isosurface pictures, and ELF calculated in the Ru–H–Ru plane for $[(\eta_6\text{-Arene})_2Ru_2(\mu_2\text{-H})_3]^+$ complex. (Reproduced with permission from Ref. [161]. Copyright 2008 American Chemistry Society.)

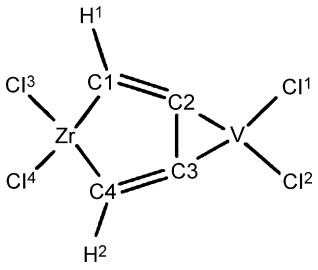

Fig. 13. Molecular structure for the model complex of $[Cp_2V(\mu\text{-}\eta^2\text{:}\eta^4\text{-butadiyne})\text{-}Zr(C_5H_4\text{-}SiMe_3)_2]$. (Reproduced with permission from Ref. [162]. Copyright 2008 American Chemistry Society.)

BCP, where the density is minimum (it coincides with the midpoint between Ru atoms) the ELF also locates a minimum, an indication that there is no electron density localized in this region.

Choukroun et al. [162] have used the ELF to elucidate the chemical bonding in a species susceptible of presenting a planar tetracoordinate carbon (ptC): $[Cp_2V(\mu\text{-}\eta^2\text{:}\eta^4\text{-butadiyne})\text{–}Zr(C_5H_4\text{–}SiMe_3)_2]$ (see Fig. 13). In Fig. 14, the ELF = 0.8 isosurface is displayed for a simplified model of the latter complex, were one can appreciate bonding basins between C2 and C3 with V and C1 and C4 with Zr. The authors proved that C1-C2-C3-C4 closely resembles *cis*-butadiene showing similar basin populations and bond lengths [162]. This case serves as an example of how tricky it may be to characterize the synaptic order from the ELF pictures. According to Fig. 14 basins lying between C1 and C2, between C3 and C4, and between C2 and C3 are apparently disynaptic. However, in Fig. 15, where basin limits are explicitly displayed, one can see how these disynaptic basins are actually trisynaptic, involving also V and Zr. Thus, the system contains three multicenter bonds: Zr–C2–C3 which is a 3c-2.2e bond, and Zr–C1–C2 and Zr–C3–C4 which are 3c-3.2e bonds. The estimation on the number of electrons has been done using the population of the basins involved. Although the molecule does not possess a ptC it contains two atoms taking part in two different three-center bonding, involving a TM.

Interesting species with multicenter bonding are the $(\eta^6\text{-arene})Cr(CO)_3$ complexes. One controversial issue in this case is how the coordination of the chromium tricarbonyl complex affects the aromaticity of the arene rings. This aspect has been the subject of a detailed investigation in the $(\eta^6\text{-}C_6H_6)Cr(CO)_3$ complex at the B3LYP/6-31G(d,p) level by Feixas et al. [163]. It is widely accepted that the structure, reactivity, and aromaticity of the benzene ring are altered significantly upon complexation with the chromium tricarbonyl complex. Thus, after coordination the ring expands, loses its planarity (the hydrogen atoms of the benzene ring slightly bent towards the $Cr(CO)_3$ fragment [164]), and shows an increased difference between alternated short and long C–C bonds [165]. The nature of the bond between the arene and the metal in $(\eta^6\text{-arene})$tricarbonylchromium complexes was discussed by Albright, Hoffmann, and coworkers some years ago [166]. These authors

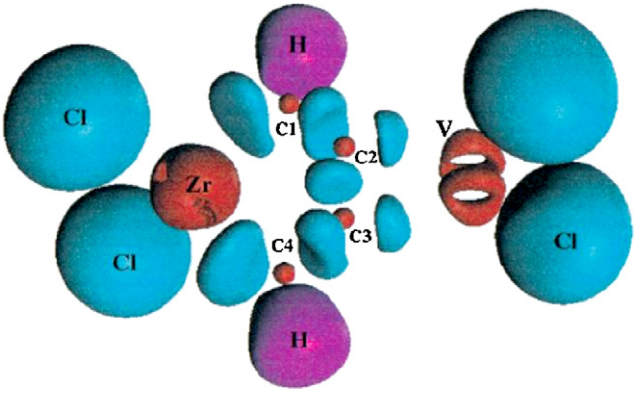

Fig. 14. Localization domains for ELF = 0.8 for model complex of $[Cp_2V(\mu\text{-}\eta^2\text{:}\eta^4\text{-butadiyne})\text{-}Zr(C_5H_4\text{-}SiMe_3)_2]$. (Reproduced with permission from Ref. [162]. Copyright 2008 American Chemistry Society.)

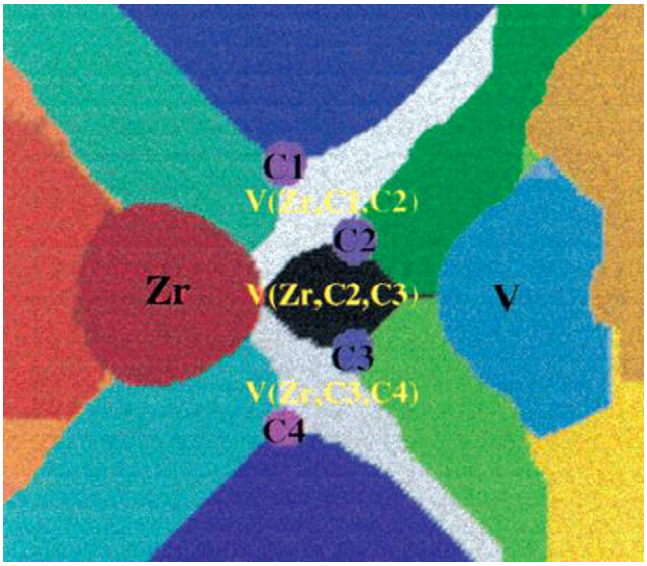

Fig. 15. Localization domains for ELF for model complex of $[Cp_2V(\mu\text{-}\eta^2\text{:}\eta^4\text{-butadiyne})\text{-}Zr(C_5H_4\text{-}SiMe_3)_2]$ given in the plane. It clearly shows the basin separations and enables an easy calculation of the synaptic order of each basin. (Reproduced with permission from Ref. [162]. Copyright 2008 American Chemistry Society.)

found that the interaction of the degenerate *2e* LUMO and $2a_1$ LUMO + 1 orbitals of the $Cr(CO)_3$ moiety with the highest occupied π-orbitals of the arene with the appropriate symmetry is the dominant bonding mechanism [167]. Charge transfer from the highest occupied π-orbitals of the arene to the lowest unoccupied *2e* and $2a_1$ orbitals of $Cr(CO)_3$ partially breaks the C–C bonds, thus explaining the observed expansion of the aromatic ring and the increase in bond length alternation for $(\eta^6\text{-}C_6H_6)Cr(CO)_3$. Because of the loss of π-electron density in the ring, one expects a partial disruption of aromaticity in the 6-MR of $(\eta^6\text{-}C_6H_6)Cr(CO)_3$ in comparison to free benzene, as discussed by Hubig et al. [165]. Indeed, all aromaticity indices used in the work [163], except NICS(0) and NICS(1), show that there is a clear reduction of the aromaticity of benzene upon coordination to the $Cr(CO)_3$ complex. This is especially clear for the indices based on the calculation of electronic delocalization. PDI, FLU, and MCI change from 0.103, 0.000, and 0.075 e in free benzene to 0.036, 0.009, and 0.019 e in complexed benzene. The failure of the NICS index to indicate loss of aromaticity due to complexation in the $(\eta^6\text{-}C_6H_6)Cr(CO)_3$ complex was due to the ring currents generated by the electron pairs that take part in the benzene–$Cr(CO)_3$ bonding. Since the claims of Mitchell et al. [168–171] about the fact that the benzene ring in tricarbonylchromium-complexed benzene is ca. 30–40% more aromatic than benzene itself were based on NICS results, these claims were considered unfounded [163].

Metallabenzenes or metallacyclohexatrienes are derived from benzene where one C–H moiety has been replaced by a fragment containing a TM [172,173]. The first stable, isolated synthesized metallabenzene was osmabenzene (osmium as TM in cyclohexatriene ring) reported by Elliot et al. in 1982 [174]. So far a plethora of metallabenzenes has been synthesized, including metallabenzenes with up to two substitutions of a C–H fragment by a TM moiety. Interestingly, TM compounds exhibit aromatic properties as already considered in the pioneering work of Thorn and Hoffmann [175]. However, it is expected that metallabenzenes will exhibit lower aromatic character than benzene due to the polarization of TM-C bonds. The ELF gives support to this view, showing a picture very close to that of benzene for C–C bonds in metallabenzenes and strong polarization in the C–TM bond [176].

4.4.2. Involving only TM

Similarly to their organic analogues such as benzene or cyclopentadienyl, metallabenzenes also stabilize upon complexation with TM, giving rise to metal sandwich complexes. Particularly interesting are these sandwich complexes in metallabenzenes, as they afford TM–TM interaction between the TM sandwiched and the TM constituting the metallabenzene. Effert et al. [176] have recently reported the synthesis of $[\{\eta^6\text{-}pd\text{Ni(Cp)}\}\text{RuCp}]^+$ and $[\{\eta^6\text{-}pd\text{Ru(CO)}_3\}_2\text{–Ru}]$ (*pd* = penta-dienylylidene) [91] and an ELF analysis of its electronic structure. In the former case, the ELF supports the bonding between the TM sandwiched and the TM in the *pd* unit by showing a disynaptic basin associated with these TMs. For the second molecule, the authors have found a trisynaptic basin involving the three ruthenium atoms in the molecule. Such a trisynaptic basin is not found in the anti conformer, which displays Ru atoms in *pd* farther from each other.

Metallic clusters are very appealing species from the point of view of the analysis of metal–metal bonding. Feliz et al. discussed the nature of bonding interactions in the $[Mo_3S_4Cl_3(PH_3)_6]^+$ cluster using DIs [177]. The authors concluded that the δ(Mo,Mo) and δ(Mo,S) values of 0.58 and about 1 e, respectively, within the $[Mo_3S_4]$ cluster core are consistent with the predominant covalent character of the Mo–Mo and Mo–S bonds. On the contrary, the δ(Mo,Cl) = 0.66 e confirms the partly ionic character of the Mo–Cl interaction. On the other hand, the ELF analysis reveals V(Mo,Cl) basin with 0.56 e of population, 88% of which is contained in Cl QTAIM atomic basin, suggesting a highly polarized bond. The bifurcation diagram shows how the $[Mo_3(\mu_3\text{-}S)(\mu_2\text{-}S)_3]$ species forms an exclusive localization domain. This domain further splits into the $[Mo_3]$ unit which consists of three disynaptic V(Mo,Mo) and one trisynaptic basin V(Mo,Mo,Mo). The $[Mo_3]$ unit holds 1.25 e. The variance of the core part of Mo atoms, C(Mo), is quite large, the main contribution coming from the basins of the sulfur atom, which suggests an Mo–μ_2–S–Mo bonding. The Mo core population (39.22 e) corresponds to the Mo^{3+} oxidation state.

Some authors from the latter work conducted another combined experimental and theoretical work [178] studying the cubane-type clusters $[Mo_3CuS_4(dmpe)_3Cl_4]^+$ and $[Mo_3NiS_4(dmpe)_3Cl_4]$. The authors analyze simplified models of these molecules by means of the ELF. The (simplified) topology of the ELF (see Fig. 16) for the $[Mo_3CuS_4]$ reveals a quite interesting chemical feature: a tetrasynaptic basin, V(Cu,Mo,Mo,Mo), involving the four TM in the cubane structure. Showing a tetrahedral disposition, these four TM behave as an independent unit. The bonding structure for this cluster is given by this four-center interaction between the TMs and the three disynaptic basins found between Mo atoms, V(Mo,Mo). Similarly, $[Mo_3NiS_4]$, shows an analogous bond pattern given by a tetrasynaptic basin V(Ni,Mo,Mo,Mo) and three disynaptic basins V(Mo,Ni). The authors also provide the covariance and the variance for the

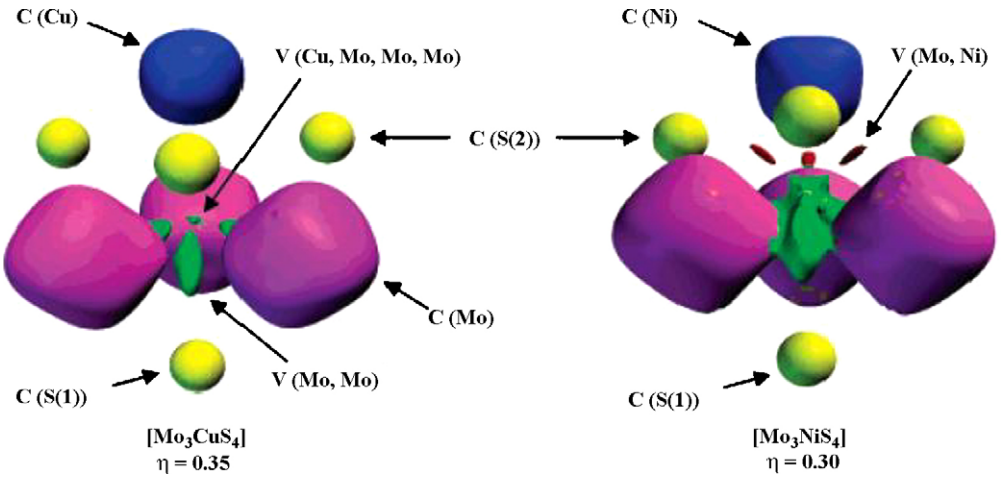

Fig. 16. Simplified valence and core attractor representation of the Mo_3MS_4 (M = Cu, Ni) units at each ELF value. (Reproduced with permission from Ref. [178]. Copyright 2008 American Chemistry Society.)

basins appearing in both systems. However, the high delocalization given in this system makes it difficult to assess which formal oxidation state is held by the TMs.

Let us analyze now the recent work of Mandado et al. [179] which discusses at the B3LYP/6-311+G(d) level the nature of the bonding in a series of all-metal clusters containing the Al_4 unit attached to an alkaline, alkaline earth, or TM using MCIs obtained from different atomic partition methods (Mulliken, QTAIM, and iterative Hirshfeld partitioning). With the QTAIM partitioning and for the C_{4v} Al_4Cu^- species, the δ(Al,Cu) and δ(Al,Al) values of 0.627 and 0.738 e are quite close to that of a single covalent bond such as, for instance, that found in the H_2 molecule. The three-center DI (3-DI) of the $CuAl_2$ unit is as large as 0.208 e, even larger than that of an Al_3 unit (0.174 e). The 4- and 5-DIs for the $CuAl_3$ and $CuAl_4$ fragments are 0.084 and 0.060 e to be compared with the values obtained for highly delocalized π-systems such as $C_4H_4^{2+}$ and $C_5H_5^-$, which are 0.180 and 0.042 e, respectively. The 4-DI of the $CuAl_3$ fragment is smaller than that found in $C_4H_4^{2+}$, yet relatively large, while the 5-DI of the $CuAl_4$ system is even larger than that of $C_5H_5^-$. Interestingly, the 4-DI in D_{4h} Al_4^{2-} species can be exactly separated into the σ and π components. The 4-DI$^\pi$ in Al_4^{2-} of 0.180 e is the same as that found for $C_4H_4^{2+}$. On the other hand, the σ component of the 4-DI is somewhat smaller (0.161 e). For the C_{4v} Al_4Cu^- species, the separation between the σ and π contributions of the 4-DI can be performed only in an approximate way by taking advantage of the fact that there is only an orbital of approximate π-symmetry. If this separation is done, it can be seen that the σ and π 4-DIs decrease significantly when going from Al_4^{2-} to Al_4Cu^-. The reduction of the 4-DI is more important in the π than in the σ system. This is an indication of an important reduction of aromaticity when going from Al_4^{2-} to Al_4Cu^-. In the case of the C_s Al_4Zn species, the Zn approaches one of the Al atoms, to which it is strongly covalently bonded. As a result, the corresponding δ(Al,Zn) is significantly larger than the rest. Also, the 3- and 4-DIs of fragments containing these two atoms are the largest ones.

In a recent paper, Ponec [180] has discussed the chemical bonding in solids by means of DIs. The author has proposed a generalization of the DI to infinite periodical structures by changing the summations over all the pairs of MSOs in Eq. (11) to integrations for the quasi-continuum of k-states in the solid state. In that way, there is a non-negligible electron delocalization coming from the interactions with distant atoms that has been attributed to "mobile" electrons in the solid. The amount of "mobile" electrons sums up to about 20% of the total delocalized electrons in idealized linear chains, and increases to 60% in an ideal square planar lattice and to 80% in a model of a simple cubic cell. Thus, the transition from simple linear chain to 3D solid is connected with the gradual built-up of the metallic character.

There are many more papers dealing with TM complexes using ELF or QTAIM approaches; it is, however, unrealistic to try to address them all here. It is not either our intention to review all the theoretical work done in the area of electron localization/delocalization of TM-complexes for which a bulky literature exists. So, we have preferred to select a series of studies that show the interest in the use of electron delocalization measures to discuss chemical bonding. However, let us finish by mentioning some topics in TM chemistry also covered by ELF and QTAIM approaches not included in this review. Dobado and coworkers have addressed the interaction of TM cations with benzene [181], and even the α-agostic bonds [182] by means of ELF and AIM. Tafipolsky and coworkers have analyzed the electron delocalization in *N*-heterocyclic carbenes containing chromium from the QTAIM viewpoint [183]. It is also worth mentioning the work of Gillespie et al. which analyzes the ELF of some complexes with non-VSPER geometries, namely MX_n (X = F, H, CH_3 and O, *M* = Ca–Mn; *n* = 2–6) which are formally d^0 species [184].

5. Summary

The electronic delocalization is central to explain structure, stability, and reactivity and to analyze the nature of bonding not only of classical organic compounds but also of many inorganic, organometallic, and all-metal cluster species. In this review, we have described a series of studies that analyze electron delocalization in transition metal complexes. Coverage has been extensive, but not exhaustive. In fact, we have confined our review effort in the studies carried out by employing two of the most widespread methods to measure delocalization: the electron localization function and the electron sharing indices obtained in the framework of the quantum theory of atoms-in-molecules. One should note that, among the several statements included in the QTAIM, in this paper we have primordially used those concerning the electron localization/delocalization and the atomic partition gathered within QTAIM framework. We have shown that the joint and complementary effort of ELF and QTAIM techniques has already been proven as one of the most powerful tools currently available in the realm of quantum chemistry to understand chemical bonding. Without doubt, these techniques are likely to be among the most extensively used quantum chemical tools to analyze chemical bonding in the future, in the field of transition metal chemistry.

Acknowledgments

The authors are grateful to Prof. Dr. Miquel Duran and Dr. Jordi Poater for helpful discussions and to the referees for valuable comments. We are indebted to Prof. Bernard Silvi for his assistance with ToPMoD package as well as for many interesting discussions during the course of our investigations with the ELF over the past years. Financial help has been furnished by the Spanish Ministerio de Educación y Ciencia (MEC) projects Nos. CTQ2005-08797-C02-01/BQU and CTQ2008-03077/BQU and by the Catalan Departament d'Universitats, Recerca i Societat de la Informació (DURSI) project No. 2005SGR-00238.

References

[1] I. Bertini, H.B. Gray, S.J. Lippard, J.S. Valentine, Bioinorganic Chemistry, Mill Valley, California, 1994.
[2] P.J. Stone, A.D. Kelman, F.M. Sinex, Nature 251 (1974) 736.
[3] T.A. Connors, J.J. Roberts (Eds.), Platinum Coordination Complexes in Chemotherapy, Springer, 1974.
[4] G. Rayner-Canham, Descriptive Inorganic Chemistry, W.H. Freeman and Company, 1996.
[5] M. Torrent, M. Solà, G. Frenking, Chem. Rev. 100 (2000) 439.
[6] G.N. Lewis, J. Am. Chem. Soc. 38 (1916) 762.
[7] E. Matito, M. Solà, P. Salvador, M. Duran, Faraday Discuss. 135 (2007) 325.
[8] C.A. Coulson, Proc. R. Soc. A 158 (1938) 413.
[9] I. Mayer, Chem. Phys. Lett. 97 (1983) 270.
[10] R.S. Mulliken, J. Chem. Phys. 23 (1955) 1833.
[11] H.A. Bethe, Ann. Phys. 3 (1929) 133.
[12] F. Weinhold, C.R. Landis, Valence and Bonding: A Natural Bond Orbital Donor-Acceptor Perspective, Cambridge U. Press, 2003.
[13] S. Dapprich, G. Frenking, J. Phys. Chem. 99 (1995) 9352.
[14] F.M. Bickelhaupt, E.J. Baerends, in: K.B. Lipkowitz, D.B. Boyd (Eds.), Reviews in Computational Chemistry, Wiley–VCH, New York, 2000, p. 1.
[15] G. Frenking, N. Frohlich, Chem. Rev. 100 (2000) 717.
[16] D.B. Chesnut, L.J. Bartolotti, Chem. Phys. 257 (2000) 175.
[17] D.B. Chesnut, L.J. Bartolotti, Chem. Phys. 278 (2002) 101.
[18] E. Matito, J. Poater, F.M. Bickelhaupt, M. Solà, J. Phys. Chem. B 110 (2006) 7189.
[19] R.F.W. Bader, G.L. Heard, J. Chem. Phys. 111 (1999) 8789.
[20] R.F.W. Bader, J. Phys. Chem. A 102 (1998) 7314.
[21] R.F.W. Bader, Chem. Eur. J. 12 (2006) 2896.
[22] J. Cioslowski, S.T. Mixon, J. Am. Chem. Soc. 114 (1992) 4382.
[23] J. Cioslowski, S.T. Mixon, Can. J. Chem. 70 (1992) 443.
[24] A. Haaland, D.J. Shorokhov, N.V. Tverdova, Chem. Eur. J. 10 (2004) 4416.
[25] A. Haaland, D.J. Shorokhov, N.V. Tverdova, Chem. Eur. J. 10 (2004) 6210.
[26] J. Poater, M. Solà, F.M. Bickelhaupt, Chem. Eur. J. 9 (2006) 1940.
[27] J. Poater, M. Sola, F.M. Bickelhaupt, Chem. Eur. J. 12 (2006) 2902.
[28] J. Poater, F.M. Bickelhaupt, M. Solà, J. Phys. Chem. A 111 (2007) 5063.
[29] J. Poater, R. Visser, M. Solà, F.M. Bickelhaupt, J. Org. Chem. 72 (2007) 1134.

[30] R.F.W. Bader, D.-C. Fang, J. Chem. Theor. Comput. 1 (2005) 403.
[31] C.F. Matta, J. Hernández-Trujillo, T.H. Tang, R.F.W. Bader, Chem. Eur. J. 9 (2003) 1940.
[32] A.M. Pendás, A. Costales, V. Luaña, J. Phys. Chem. B 102 (1998) 6937.
[33] A.M. Pendás, E. Francisco, M.A. Blanco, C. Gatti, Chem. Eur. J. 13 (2007) 9362.
[34] J. Hernández-Trujillo, I. García-Cruz, J.M. Martínez-Magadán, Chem. Phys. 308 (2005) 181.
[35] M. Kohout, Faraday Discuss. 135 (2007) 43.
[36] R.F.W. Bader, Acc. Chem. Res. 18 (1985) 9.
[37] R.F.W. Bader, Atoms in Molecules: A Quantum Theory, Clarendon, Oxford, 1990.
[38] R.F.W. Bader, Chem. Rev. 91 (1991) 893.
[39] The Quantum Theory of Atoms in Molecules. From Solid State to DNA and Drug Design, Wiley–VCH Verlag GmbH & Co. KGaA, Weinheim, 2007.
[40] R.F.W. Bader, P.J. MacDougall, C.D.H. Lau, J. Am. Chem. Soc. 106 (1984) 1594.
[41] R.F.W. Bader, Can. J. Chem. 76 (1998) 973.
[42] R.F.W. Bader, C. Chang, J. Phys. Chem. 93 (1989) 2946.
[43] P.J. MacDougall, M.B. Hall, in: R. Blessing (Ed.), Transactions of the American Crystallographic Association, American Crystallographic Association, New York, 1990, p. 105.
[44] W. Scherer, P. Sirsch, M. Grosche, M. Spiegler, S.A. Mason, M.G. Gardiner, Chem. Commun. (2001) 2072.
[45] W. Scherer, P. Sirsch, D. Shorokhov, M. Tafipolsky, G.S. McGrady, E. Gullo, Chem. Eur. J. 9 (2003) 6057.
[46] P. Macchi, A. Sironi, Coord. Chem. Rev. 238–239 (2003) 383.
[47] M. Solà, J. Mestres, R. Carbó, M. Duran, J. Chem. Phys. 104 (1996) 636.
[48] R.F.W. Bader, S. Johnson, T.H. Tang, P.L.A. Popelier, J. Phys. Chem. 100 (1996) 15398.
[49] E.R. Davidson, Reduced Density Matrices in Quantum Chemistry, Academic, New York, 1976.
[50] R. McWeeny, Methods of Molecular Quantum Mechanics, Academic, London, 1976.
[51] A.J. Coleman, Int. J. Quantum Chem. 85 (2001) 196.
[52] J. Cioslowski, Many-Electron Densities and Reduced Density Matrices, Kluwer Academic/Plenum Publishers, New York, 2000.
[53] R.F.W. Bader, M.E. Stephens, Chem. Phys. Lett. 26 (1974) 445.
[54] R.F.W. Bader, M.E. Stephens, J. Am. Chem. Soc. 97 (1975) 7391.
[55] E.J. Baerends, O.V. Gritsenko, J. Phys. Chem. A 101 (1997) 5383.
[56] M.A. Buijse, E.J. Baerends, in: D.E. Ellis (Ed.), Density Functional Theory of Molecules, Clusters and Solids, Kluwer, Dordrecht, 1995, p. 1.
[57] M.A. Buijse, E.J. Baerends, Mol. Phys. 100 (2002) 401.
[58] C. Bo, J.P. Sarasa, J.M. Poblet, J. Phys. Chem. 97 (1993) 6362.
[59] K.E. Laidig, L.M. Cameron, J. Am. Chem. Soc. 118 (1996) 1737.
[60] X. Fradera, M.A. Austen, R.F.W. Bader, J. Phys. Chem. A 103 (1999) 304.
[61] X. Fradera, J. Poater, S. Simon, M. Duran, M. Solà, Theor. Chem. Acc. 108 (2002) 214.
[62] P.L.A. Popelier, Atoms in Molecules: An Introduction, Prentice Hall, Harlow, 2000.
[63] R. Ponec, J. Math. Chem. 21 (1997) 323.
[64] R. Ponec, A.J. Duben, J. Comput. Chem. 20 (1999) 760.
[65] R. Ponec, J. Roithová, Theor. Chem. Acc. 105 (2001) 383.
[66] R. Ponec, J. Roithová, X. Gironés, K. Jug, J. Mol. Struct. (Theochem) 545 (2001) 255.
[67] R. Ponec, J. Roithová, X. Gironés, L. Lain, A. Torre, R. Bochicchio, J. Phys. Chem. A 106 (2002) 1019.
[68] R. Ponec, G. Yuzhakov, R. Carbó-Dorca, J. Comput. Chem. 24 (2003) 1829.
[69] R. Ponec, G. Yuzhakov, X. Gironés, G. Frenking, Organometallics 23 (2004) 1790.
[70] R. Ponec, G. Lendvay, J. Chaves, J. Comput. Chem. 29 (2008) 1387.
[71] F.M. Bickelhaupt, M. Solà, C. Fonseca-Guerra, J. Chem. Theor. Comput. 2 (2006) 965.
[72] M.J.S. Dewar, Bull. Soc. Chim. Fr. (Paris) 18 (1951) C79.
[73] J. Chatt, J.S. Duncanson, J. Chem. Soc. (1953) 2929.
[74] I. Mayer, P. Salvador, Chem. Phys. Lett. 383 (2004) 368.
[75] E. Matito, J. Poater, M. Solà, M. Duran, P. Salvador, J. Phys. Chem. A 109 (2005) 9904.
[76] E. Matito, P. Salvador, M. Duran, M. Solà, J. Phys. Chem. A 110 (2006) 5108.
[77] J. Poater, M. Solà, M. Duran, X. Fradera, Theor. Chem. Acc. 107 (2002) 362.
[78] F.W. Biegler-König, R.F.W. Bader, T.-H. Tang, J. Comput. Chem. 3 (1982) 317, http://www.chemistry.mcmaster.ca/aimpac/.
[79] F.W. Biegler-König, J. Comput. Chem. 21 (2000) 1040.
[80] F.W. Biegler-König, J. Schönbohm, D. Bayles, J. Comput. Chem. 22 (2001) 545.
[81] F.W. Biegler-König, J. Schönbohm, J. Comput. Chem. 23 (2002) 1489.
[82] P.L.A. Popelier, Comput. Phys. Commun. 93 (1996) 212.
[83] P.L.A. Popelier, MORPHY98 UMIST, Manchester, England, 1998.
[84] N.O.J. Malcolm, P.L.A. Popelier, J. Comput. Chem. 24 (2003) 1276.
[85] J.C. Ortíz, C. Bo, Xaim Universitat Rovira i Virgili, Tarragona.
[86] C. Gatti, V.R. Saunders, C. Roetti, J. Chem. Phys. 101 (1994) 10686.
[87] M.J. Frisch, G.W. Trucks, H.B. Schlegel, G.E. Scuseria, M.A. Robb, J.R. Cheeseman, V.G. Zakrzewski, J.A. Montgomery, R.E. Stratmann, J.C. Burant, S. Dapprich, J.M. Millam, A.D. Daniels, K.N. Kudin, M.C. Strain, O. Farkas, J. Tomasi, V. Barone, M. Cossi, R. Cammi, B. Mennucci, C. Pomelli, C. Adamo, S. Clifford, J. Ochterski, G.A. Petersson, P.Y. Ayala, Q. Cui, K. Morokuma, P. Salvador, J.J. Dannenberg, D.K. Malick, A.D. Rabuck, K. Raghavachari, J.B. Foresman, J. Cioslowski, J.V. Ortiz, A.G. Baboul, B.B. Stefanov, G. Liu, A. Liashenko, P. Piskorz, I. Komaromi, R. Gomperts, R.L. Martin, D.J. Fox, T. Keith, M. Al-Laham, C. Peng, A. Nanayakkara, M. Challacombe, P.M.W. Gill, B.G. Johnson, W. Chen, M.W. Wong, J.L. Andres, R. Gonzalez, M. Head-Gordon, E.S. Replogle, J.A. Pople, Gaussian 98, Pittsburgh, PA, 1998.
[88] M. Giambiagi, M.S. de Giambiagi, C.D. dos Santos, A.P. de Figueiredo, Phys. Chem. Chem. Phys. 2 (2000) 3381.
[89] M. Giambiagi, M.S. de Giambiagi, K.C. Mundim, Struct. Chem. 1 (1990) 423.
[90] J. Cioslowski, E. Matito, M. Solà, J. Phys. Chem. A 111 (2007) 6521.
[91] J. Poater, X. Fradera, M. Duran, M. Solà, Chem. Eur. J. 9 (2003) 400.
[92] E. Matito, M. Duran, M. Solà, J. Chem. Phys. 122 (2005) 014109.
[93] P. Bultinck, R. Ponec, S. Van Damme, J. Phys. Org. Chem. 18 (2005) 706.
[94] E. Matito, M. Solà, M. Duran, J. Poater, J. Mol. Struct. (Theochem) 727 (2005) 165.
[95] F. Feixas, E. Matito, J. Poater, M. Solà, J. Comput. Chem. 29 (2008) 1543.
[96] E. Matito, ESI-3D: Electron Sharing Indexes Program for 3D Molecular Space Partitioning. IQC, Girona, 2006, available from http://iqc.udg.es/~eduard/ESI.
[97] A.J. Bridgeman, G. Cavigliasso, L.R. Ireland, J. Rothery, J. Chem. Soc., Dalton Trans. (2001) 2095.
[98] J. Poater, M. Duran, M. Solà, B. Silvi, Chem. Rev. 105 (2005) 3911.
[99] F. Cortés-Guzmán, R.F.W. Bader, Coord. Chem. Rev. 249 (2005) 633.
[100] A.D. Becke, K.E. Edgecombe, J. Chem. Phys. 92 (1990) 5397.
[101] A. Savin, R. Nesper, S. Wengert, T.F. Fassler, Angew. Chem., Int. Ed. Engl. 36 (1997) 1809.
[102] A. Savin, A.D. Becke, J. Flad, R. Nesper, H. Preuss, H.G. Vonschnering, Angew. Chem., Int. Ed. Engl. 30 (1991) 409.
[103] B. Silvi, A. Savin, Nature 371 (1994) 683.
[104] A.D. Becke, Int. J. Quantum Chem. 23 (1983) 1915.
[105] P.O. Löwdin, Phys. Rev. 97 (1955) 1474.
[106] B. Silvi, J. Phys. Chem. A 107 (2003) 3081.
[107] M. Kohout, Int. J. Quantum Chem. 97 (2004) 651.
[108] J.F. Dobson, J. Chem. Phys. 94 (1991) 4328.
[109] J.F. Dobson, J. Chem. Phys. 98 (1993) 8870.
[110] E. Matito, B. Silvi, M. Duran, M. Solà, J. Chem. Phys. 125 (2006) 024301.
[111] A. Savin, J. Mol. Struct. (Theochem) 727 (2007) 127.
[112] J. Melin, P. Fuentealba, Int. J. Quantum Chem. 92 (2003) 381.
[113] J.C. Santos, J. Andrés, A. Aizman, P. Fuentealba, J. Chem. Theor. Comput. 1 (2005) 83.
[114] J.C. Santos, W. Tiznado, R. Contreras, P. Fuentealba, J. Chem. Phys. 120 (2004) 1670.
[115] X. Krokidis, S. Noury, B. Silvi, J. Phys. Chem. A 101 (1997) 7277.
[116] S. Berski, J. Andrés, B. Silvi, L.R. Domingo, J. Phys. Chem. A 107 (2003) 6014.
[117] E. Matito, M. Solà, M. Duran, J. Poater, J. Phys. Chem. B 109 (2005) 7591.
[118] E. Matito, J. Poater, M. Duran, M. Solà, Chemphyschem 7 (2006) 111.
[119] T.F. Fassler, A. Savin, Chem. Unserer Zeit 31 (1997) 110.
[120] M. Kohout, A. Savin, Int. J. Quantum Chem. 60 (1996) 875.
[121] M. Kohout, A. Savin, J. Comput. Chem. 18 (1997) 1431.
[122] H. Schmider, R.P. Sagar, V.H. Smith, J. Chem. Phys. 94 (1991) 8627.
[123] R.P. Sagar, A.C.T. Ku, VHS Jr., J. Chem. Phys. 88 (1988) 4387.
[124] M. Kohout, A. Savin, H. Preuss, J. Chem. Phys. 95 (1991) 1928.
[125] A. Savin, B. Silvi, F. Colonna, Can. J. Chem. 74 (1996) 1088.
[126] B. Silvi, Phys. Chem. Chem. Phys. 6 (2004) 256.
[127] J. Pilme, B. Silvi, M.E. Alikhani, J. Phys. Chem. A 109 (2005) 10028.
[128] S. Noury, X. Krokidis, F. Fuster, B. Silvi, TopMod Package, 1997.
[129] J. Poater, M. Solà, A. Rimola, L. Rodríguez-Santiago, M. Sodupe, J. Phys. Chem. A 108 (2004) 6072.
[130] J. Poater, M. Duran, M. Solà, J. Comput. Chem. 22 (2001) 1666.
[131] M. Güell, J.M. Luis, L. Rodríguez-Santiago, M. Sodupe, M. Solà, J. Phys. Chem. A (submitted for publication).
[132] J. Poater, M. Sodupe, J. Bertran, M. Solà, Mol. Phys. 103 (2005) 163.
[133] P.v.R. Schleyer, C. Maerker, A. Dransfeld, H. Jiao, N.J.R. van Eikema Hommes, J. Am. Chem. Soc. 118 (1996) 6317.
[134] J. Kruszewski, T.M. Krygowski, Tetrahedron Lett. 13 (1972) 3839.
[135] M.K. Cyrański, M. Gilski, M. Jaskolski, T.M. Krygowski, J. Org. Chem. 68 (2003) 8607.
[136] V.G.S. Box, F. Jean-Mary, J. Mol. Model. 7 (2001) 334.
[137] A.H. Pakiari, M. Farrokhnia, S.M. Azami, Chem. Phys. Lett. 457 (2008) 211.
[138] J.A. Dobado, J. Molina Molina, R. Uggla, M.R. Sundberg, Inorg. Chem. 39 (2000) 2831.
[139] R.F.W. Bader, C.F. Matta, Inorg. Chem. 40 (2001) 5603.
[140] J. Poater, M. Cases, X. Fradera, M. Duran, M. Solà, Chem. Phys. 294 (2003) 129.
[141] R. Bochicchio, R. Ponec, A. Torre, L. Lain, Theor. Chem. Acc. 105 (2001) 292.
[142] A.B. Sannigrahi, T. Kar, Chem. Phys. Lett. 173 (1990) 569.
[143] K.C. Mundim, M. Giambiagi, M.S. de Giambiagi, J. Phys. Chem. 98 (1994) 6118.
[144] T. Kar, E. Sánchez-Marcos, Chem. Phys. Lett. 192 (1992) 14.
[145] R. Ponec, I. Mayer, J. Phys. Chem. A 101 (1997) 1738.
[146] J. Pilme, B. Silvi, M.E. Alikhani, J. Phys. Chem. A 107 (2003) 4506.
[147] P. Macchi, L. Garlaschelli, A. Sironi, J. Am. Chem. Soc. 124 (2002) 14173.
[148] P. Macchi, A. Sironi, in: C.F. Matta, R.J. Boyd (Eds.), The Quantum Theory of Atoms in Molecules From Solid State to DNA and Drug Design, Wiley–VCH, Weinheim, 2007.
[149] F.A. Cotton, G. Wilkinson, Advanced Inorganic Chemistry, John Wiley & Sons Inc., New York, 1980.
[150] L.H. Gade, Angew. Chem., Int. Ed. Engl. 39 (2000) 2658.
[151] G. Jansen, M. Schubart, B. Findeis, L.H. Gade, I.J. Scowen, M. McPartlin, J. Am. Chem. Soc. 120 (1998) 7239.

[152] M. Kohout, F.R. Wagner, Y. Grin, Theor. Chem. Acc. 108 (2002) 150.
[153] M. Yu, M. Dolg, Chem. Phys. Lett. 273 (1997) 329.
[154] L.J. Farrugia, Chem. Phys. Lett. 414 (2005) 122.
[155] H. Chevreau, C. Martinsky, A. Sevin, C. Minot, B. Silvi, New J. Chem. 27 (2003) 1049.
[156] P. Macchi, D. Donghi, A. Sironi, J. Am. Chem. Soc. 127 (2005) 16494.
[157] R. Ponec, G. Yuzhakov, Theor. Chem. Acc. 118 (2007) 791.
[158] P. Laszlo, Angew. Chem., Int. Ed. Engl. 39 (2000) 2071.
[159] H. Braunschweig, M. Colling, Coord. Chem. Rev. 223 (2001) 1.
[160] H. Braunschweig, K. Radacki, D. Rais, F. Seeler, Angew. Chem., Int. Ed. Engl. 45 (2006) 1066.
[161] E.P. Fowe, B. Therrien, G. Süss-Fink, C. Daul, Inorg. Chem. 47 (2008) 42.
[162] R. Choukroun, B. Donnadieu, J.S. Zhao, P. Cassoux, C. Lepetit, B. Silvi, Organometallics 19 (2000) 1901.
[163] F. Feixas, J.O.C. Jiménez-Halla, E. Matito, J. Poater, M. Solà, Polish J. Chem. 81 (2007) 783.
[164] A.A. Low, M.B. Hall, Int. J. Quantum Chem. 77 (2000) 152.
[165] S.M. Hubig, S.V. Linderman, J.K. Kochi, Coord. Chem. Rev. 200–202 (2006) 831.
[166] T.A. Albright, P. Hoffmann, R. Hoffmann, C.P. Lillya, P.A. Dobosh, J. Am. Chem. Soc. 105 (1983) 3396.
[167] A. Arrais, E. Diana, G. Gervasio, R. Gobbeto, D. Marabello, P.L. Stanghellini, Eur. J. Inorg. Chem. (2004) 1505.
[168] R.H. Mitchell, Chem. Rev. 101 (2001) 1301.
[169] R.H. Mitchell, Z. Brkic, D.J. Berg, T.M. Barclay, J. Am. Chem. Soc. 124 (2002) 11983.
[170] R.H. Mitchell, Y. Chen, N. Khalifa, P. Zhou, J. Am. Chem. Soc. 120 (1998) 1785.
[171] R.H. Mitchell, P. Zhou, S. Venugopalan, T.W. Dingle, J. Am. Chem. Soc. 112 (1990) 7812.
[172] J.R. Bleeke, Chem. Rev. 101 (2001) 1205.
[173] I. Fernández, G. Frenking, Chem. Eur. J. 13 (2007) 5873.
[174] G.P. Elliot, W.R. Roper, J.M. Waters, J. Chem. Soc., Chem. Commun. (1982) 811.
[175] D.L. Thorn, R. Hoffmann, Nouv. J. Chem. 3 (1979) 39.
[176] U. Effertz, U. Englert, F. Podewils, A. Salzer, T. Wagner, M. Kaupp, Organometallics 22 (2003) 264.
[177] M. Feliz, R. Llusar, J. Andrés, S. Berski, B. Silvi, New J. Chem. 26 (2002) 844.
[178] J. Andrés, M. Feliz, J. Fraxedas, V. Hernández, J.T. López-Navarrete, R. Llusar, G. Sauthier, F.R. Sensato, B. Silvi, C. Bo, J.M. Campanera, Inorg. Chem. 46 (2007) 2159.
[179] M. Mandado, A. Krishtal, C. Van Alsenoy, P. Bultinck, J.M. Hermida-Ramón, J. Phys. Chem. A 111 (2007) 11885.
[180] R. Ponec, Theor. Chem. Acc. 114 (2005) 208.
[181] J. Molina, J. Dobado, S. Melchor, J. Mol. Struct. (Theochem) 589–590 (2002) 337.
[182] I. Vidal, S. Melchor, I. Alkorta, J. Elguero, M.R. Sundberg, J.A. Dobado, Organometallics 25 (2006) 5638.
[183] M. Tafipolsky, W. Scherer, K. Öfele, G. Artus, B. Pedersen, W. Herrmann, G.S. McGrady, J. Am. Chem. Soc. 124 (2002) 5865.
[184] R. Gillespie, S. Noury, J. Pilme, B. Silvi, Inorg. Chem. 43 (2004) 3248.
[185] R. Pou-Amerigo, M. Merchan, I. Nebot-Gil, P.O. Widmark, B. Roos, Theor. Chim. Acta 92 (1995) 149.